ELECTRONIC SUPPLEMENTARY INFORMATION

Engineering macrocyclic high performance pentagonal bipyramidal Dy(III) single-ion magnets†

Angelos B. Canaj,[a] Sourav Dey,[b] Claire Wilson[a], Oscar Cespedes,[c] Gopalan Rajaraman*[b] and Mark Murrie*[a]

[a] School of Chemistry, University of Glasgow, University Avenue, Glasgow, G12 8QQ, UK. E-mail: Mark.Murrie@glasgow.ac.uk

[b] Department of Chemistry, Indian Institute of Technology Bombay, Powai, Mumbai, Maharashtra, 400076, India. E-mail: rajaraman@chem.iitb.ac.in

[c] School of Physics and Astronomy, University of Leeds, Leeds LS2 9JT, UK.

Abstract. We generate a new air-stable *pseudo*-D_{5h} Dy(III) Single-Molecule Magnet (U_{eff} = 1108 K, T_B = 14 K) by combining a weak equatorial ligand field from a macrocyclic L^{N5} ligand with a strong axial ligand field. Based on our synthetic blueprint, we use *ab initio* calculations to show the vast scope for macrocyclic engineering of magnetic anisotropy.

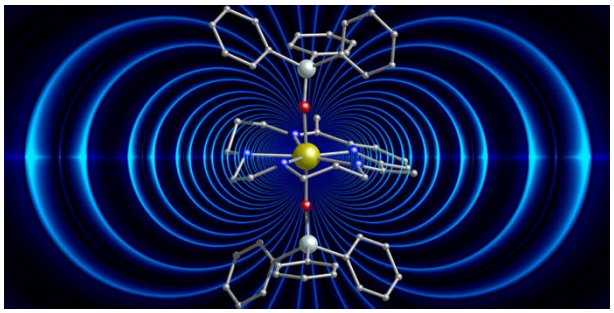

Table of Contents

1. Materials and physical measurements

All experiments were carried under aerobic conditions using materials and solvents as received without further purification. Elemental analyses (C, H, N) were performed by the University of Glasgow microanalysis service. Variable-temperature, solid-state direct current (dc) magnetic susceptibility data were collected on a Quantum Design MPMS-XL SQUID magnetometer equipped with a 5 T magnet at the University of Glasgow and on a Quantum Design SQUID-VSM magnetometer at the University of Leeds. Ac magnetic susceptibility data were collected on a Quantum Design MPMS-XL SQUID magnetometer and a Quantum Design MPMS3 SQUID magnetometer at the University of Glasgow. Microcrystalline samples were prepared using a mortar and pestle in open air and then added to gelatin capsules in the presence of eicosane. Diamagnetic corrections were applied to the observed paramagnetic susceptibilities using Pascal's constants. The diamagnetic contribution of the sample holder and eicosane were corrected by measurements. Powder XRD measurements were collected on freshly prepared samples of $[Dy^{III}(L^{N5})(Ph_3SiO)_2](BPh_4)\cdot CH_2Cl_2$ (**1**) on a PANalytical X'Pert Pro MPD diffractometer (λ (CuKα_1) = 1.5405 Å) on a mounted bracket sample stage, at the University of Glasgow. Single Crystal X-Ray diffraction data were collected using a Bruker D8 VENTURE diffractometer equipped with a Photon II CPAD detector, with an Oxford Cryosystems N-Helix device mounted on an IμS 3.0 (dual Cu and Mo) microfocus sealed tube generator at the University of Glasgow.

2. Synthesis and characterization

Synthetic strategy for **$Dy^{III}(L^{N5})(Ph_3SiO)_2](BPh_4)\cdot CH_2Cl_2$** (**1**)*:*

N,N'-Bis(3-aminopropyl)ethylenediamine (0.73 ml, 4 mmol), $DyCl_3\cdot 6H_2O$ (754 mg, 2 mmol) and 2,6-Diacetylpyridine (652 mg, 4 mmol) were transferred in a round bottom flask containing 50 ml of MeOH. The light yellow coloured reaction mixture was then refluxed for 24 hours giving a brown solution without any precipitation present. Evaporation of the MeOH solvent using a rotary evaporator yields an oily precipitate. The oily precipitate was transferred (~ 30 mg) into a 20 ml conical flask containing Ph_3SiOH (55 mg, 0.2 mmol), $NaBPh_4$ (17mg 0.05 mmol), 5 ml of distilled water and 5 ml of dichlormethane (DCM), creating two layers. The reaction mixture was heated at 100 °C in a fumehood until the DCM layer was evaporated. Then the H_2O layer was allowed to cool to room

temperature. Another 5ml of DCM was added and the two layers are stirred for 10 min. The DCM layer was separated, filtered and block like prismatic single crystals suitable for X-ray structure determination of $[Dy^{III}(L^{N5})(Ph_3SiO)_2](BPh_4)\cdot CH_2Cl_2$ (**1**) were isolated after 5-7 days by layering the DCM solution with hexane.

Elemental Anal. calcd. (found) for **1**·0.45C_6H_{14}·0.15H_2O: C 66.03 (66.37), H 5.61 (5.91), N 4.94 (4.8) %.

Crystallographic details

The structure of **1** was solved using ShelXT (SHELXT: Sheldrick, G. M. (2015). Acta Cryst. A71, 3-8.) and refined using ShelXL (Sheldrick, G.M. (2015). Acta Cryst. C71, 3-8) within the program Olex2 (Dolomanov, O.V., Bourhis, L.J., Gildea, R.J, Howard, J.A.K. & Puschmann, H. (2009), J. Appl. Cryst. 42, 339-341). Positional parameters and anisotropic atomic displacement parameters (adps) were refined for all non-Hydrogen atoms except for a number of macrocycle atoms which were refined over two partially occupied positions (0.5:0.5 and 0.6:0.4 for each ligand) as part of a disorder model, where isotropic adps were retained. Suitable distance and adp similarity restraints were applied to these atoms. Hydrogen atoms were placed in calculated positions and included as part of a riding model except for the Me hydrogen atoms which were included as rigid rotors. The full details are available in the CIF (CCDC 2000246).

Table S1. The family of Dy(III) SIMs with the pentagonal bipyramidal geometry.

Complex	U_{eff} (K)	τ_0 (s)	H_{dc} (Oe)	C ($s^{-1} K^{-n}$)	n	Calcd U_{cal} (K)	FC/ZFC Divergence (K)	Hysteresis open to (K)	sweep rate (T/s)	Ref
$Dy^{III}(L^{N5})(Ph_3SiO)_2](BPh_4)\cdot CH_2Cl_2$	**1108**	**$1.56\cdot10^{-11}$**	**0**	**0.03**	**2.05**	**1040**	**7**	**14**	**0.01**	**This work**
$[Dy(Cy_3PO)_2(H_2O)_5]Cl_3\cdot(Cy_3PO)\cdot H_2O\cdot EtOH$	472	$8.70\cdot10^{-12}$	0	N/A	N/A	430	8	11	0.02	1
$[Dy(Cy_3PO)_2(H_2O)_5]Br_3\cdot2(Cy_3PO)\cdot2H_2O\cdot2EtOH$	543	$2.00\cdot10^{-11}$	0	N/A	N/A	397	11	20	0.02	1
$[(L^1)_2Dy(H_2O)_5][I]_3(L^1)_2(H_2O)$	651.0	$5.63\cdot10^{-12}$	0	0.000692	3	688.3	12	12	0.0018	2
[Dy(bbpen)Cl]	708	$9.46\cdot10^{-11}$	0	N/A	N/A	843	7.5	8	0.02	3
[Dy(bbpen)Br]	1025	$4.21\cdot10^{-12}$	0	N/A	N/A	1037	9.5	14	0.02	3
$[Dy(O^tBu)_2(py)_5][BPh_4]$	1815	$1.17\cdot10^{-12}$	0	$1\cdot10^{-6}$	3.77	1755	14	8.8	0.012	4
$[Dy(bbpen\text{-}CH_3)Cl]$	723	$2.36\cdot10^{-10}$	0	0.00460	2.97	N/A	7.7	9	0.02	5
$[Dy(bbpen\text{-}CH_3)Br]$	1162	$1.02\cdot10^{-12}$	0	0.000535	3.15	1179	12.1	15	0.02	5
$[Dy(Bpen)(Cl)_3]$ (1)	22	$3.72\cdot10^{-06}$	800	N/A	N/A	53	N/A	N/A	N/A	5
$[Dy(Bpen)Cl(OphCl_2NO_2)_2]$	86	$4.65\cdot10^{-07}$	1000	N/A	N/A	442	N/A	N/A	N/A	6
$[Dy(Bpen)(OphCl_2NO_2)_3]$	34	$2.40\cdot10^{-06}$	800	N/A	N/A	314	N/A	N/A	N/A	6
$[Dy(Bpen)(OphNO_2)_3]$	27	$1.12\cdot10^{-06}$	800	N/A	N/A	336	N/A	N/A	N/A	6
$[Dy(H_2O)_5(HMPA)_2]Cl_3\cdot HMPA\cdot H_2O$	460	$2\cdot10^{-11}$	0	N/A	N/A	586	7	6	0.004	7
$[Dy(H_2O)_5(HMPA)_2]I_3\cdot2HMPA$	600	$1.2\cdot10^{-11}$	0	N/A	N/A	640	8	9	0.004	7
$[Dy(THF)_5Cl_2][BPh_4]$ 0.5(THF)	83	$4.1\cdot10^{-10}$	0	0.038	5	N/A	N/A	N/A	N/A	8
$[Dy(Hbpen)Cl(OPhBr_2NO_2)_2]$	181.7	$6.28\cdot10^{-7}$	0	10.75	2.08	N/A	N/A	2.5	0.02	9
$[Dy(OPCy_3)_2(H_2O)_5](CF_3SO_3)_3\cdot2OPCy$	562	$1.7\cdot10^{-11}$	0	N/A	N/A	732	8.5	2	0.018	10
$[Dy(^tBuO)Cl(THF)_5][BPh_4]\cdot2THF$	950	$3\cdot10^{-12}$	0	$2\cdot10^{-6}$	4.6	N/A	7	N/A	N/A	11
$[(NCN)DyCl_2(THF)_2]$	335.2	$6\cdot10^{-10}$	0	N/A	N/A	377	N/A	1.9	N/A	12
$[Dy(OCMe_3)Cl(THF)_5]BPh_4$	938	-11.36 [a]	0	$10^{-5.75}$	4.5	808	7	11.0	0.0015	13
$[Dy(OSiMe_3)Cl(THF)_5]BPh_4$	800	-10.55 [a]	0	$10^{-5.19}$	4.2	807	4.5	9.0	0.0015	13
$[Dy(OCMe_3)Br(THF)_5]BPh_4$	818	-10.77 [a]	0	$10^{-4.35}$	3.7	802	4.5	9.0	0.0015	13
$[Dy(OSiMe_3)Br(THF)_5]BPh_4$	732	-10.97 [a]	0	$10^{-5.18}$	4.5	680	4.5	9.0	0.0015	13
$[Dy(OPh)Cl(THF)_5]BPh_4$	736	-10.35 [a]	0	$10^{-4.82}$	4.1	584	6.8	9.0	0.0015	13
$[Dy(OPh)_2(THF)_5]BPh_4$	1329	-11.31 [a]	0	$10^{-5.99}$	4.0	1227	12	18.0	0.0015	13
$Dy(OPh)_2(py)_5]BPh_4$	1301	-12.44 [a]	0	$10^{-5.39}$	4.2	1188	13	16.0	0.0015	13
$[Dy(OCMe_3)_2(py)_5]BPh_4$	1805	-11.86 [a]	0	$10^{-5.79}$	3.6	1701	14	25.0	0.0015	13

$[Dy(OSiMe_3)_2(py)_5]BPh_4$	1595	-11.81 [a]	0	$10^{-6.54}$	4.1	1583	15	22.0	0.0015	13
$[Dy(OSiMe_3)_2(4\text{-}Mepy)_5]BPh_4$	1497.8	-11.52 [a]	0	$10^{-5.78}$	3.6	1542	16	23.0	0.0015	13
$[Zn_2Dy(L^3)_2MeOH]NO_3\cdot 3MeOH\cdot H_2O$	439	N/A	0	N/A	N/A	424	N/A	11	0.02	14
$M_{10-x}Dy_x(PO_4)_6(OH_{1-x/2})_2$ (M=Ca, X=0.5)	1140	$1.1\cdot10^{-12}$	0	$7\cdot10^{-5}$	4.36	N/A	11	1.8	0.005	15
$M_{10-x}Dy_x(PO_4)_6(OH_{1-x/2})_2$ (M=Ca, X=1)	1128	$1.5\cdot10^{-12}$	0	$4.3\cdot10^{-5}$	4.50	1130.9	N/A	N/A	N/A	15
$M_{10-x}Dy_x(PO_4)_6(OH_{1-x/2})_2$ (M=Sr, X=0.1)	1474.8	$1.3\cdot10^{-13}$	0	$8\cdot10^{-6}$	4.35	1470.44	4.5	1.8	0.005	15
$M_{10-x}Dy_x(PO_4)_6(OH_{1-x/2})_2$ (M=Sr, X=0.2)	1500.7	$1.0\cdot10^{-13}$	0	$7\cdot10^{-6}$	4.39	N/A	N/A	N/A	N/A	15

a: these parameters are log[τ0(s)] as given from ref 13.

Cy_3PO = tricyclohexyl phosphine oxide, L^1 = (^{t}BuPO(NH^{i}Pr)$_2$), H_2bbpen = *N,N'*-bis(2-hydroxybenzyl)-*N,N'*-bis(2-methylpyridyl)ethylenediamine),), Bpen = *N,N'*-bis(2-methylenepyridinyl)etyhlenediamine, $HOPhCl_2NO_2$ = 2,6-dichloro-4-nitrophenol, $HOPhNO_2$ = *p*-nitrophenol, HMPA = hexamethylphosphoramide, Hbpen = N,N′-bis(2-pyridylmethyl)-ethylenediamine,

Table S2. Crystallographic data for complex **1**.

	1
Formula	$C_{78}H_{79}DyCl_2BN_5O_2Si_2$
M_W/g mol^{-1}	1418.85
Crystal System	Triclinic
Space group	*P*-1
a/Å	14.3753 (11)
b/Å	22.1443 (17)
c/Å	22.1443 (17)
α/^{o}	100.425 (3)
β/^{o}	103.832 (3)
γ/^{o}	100.857 (3)
V/Å^3	4545.6 (4)
Z	4
T/K	150
λ/Å	0.71073
θ range for data collection/ ^{o}	2.2–28.0
D_c/g cm^{-3}	1.364
μ(Mo-K$_\alpha$)/ mm^{-1}	1.24
Meas./indep.(R_{int}) refl.	103339/32846 (0.040)
Obs. refl. [$I>2\sigma(I)$]	24960
$wR(F^2)$	0.199
$R[F^2 > 2s(F^2)]$	0.068
S	1.05
$\Delta\rho_{max,min}$/ eÅ^{-3}	5.19, -1.91

Table S3. Selected bond distances and angles for complex **1** (Å, º).

Dy1A—O1A	2.157 (3)	Dy1B—O1B	2.161 (4)
Dy1A—O2A	2.136 (4)	Dy1B—O2B	2.158 (4)
Dy1A—N1A	2.400 (5)	Dy1B—N1B	2.457 (5)
Dy1A—N2A	2.570 (5)	Dy1B—N2B	2.564 (5)
Dy1A—N5A	2.462 (6)	Dy1B—N4B	2.541 (6)
Dy1A—N3A	2.537 (9)	Dy1B—N5B	2.460 (5)
Dy1A—N4A	2.508 (8)	Dy1B—N3B	2.558 (12)
O1A—Dy1A—N1A	85.07 (14)	O1B—Dy1B—N1B	80.71 (15)
O1A—Dy1A—N2A	93.03 (15)	O1B—Dy1B—N2B	88.47 (16)
O1A—Dy1A—N5A	90.5 (2)	O1B—Dy1B—N4B	81.2 (2)
O1A—Dy1A—N3A	91.7 (4)	O1B—Dy1B—N5B	93.63 (17)
O1A—Dy1A—N4A	82.9 (3)	O1B—Dy1B—N3B	92.8 (3)
O2A—Dy1A—O1A	176.54 (15)	O2B—Dy1B—O1B	173.13 (15)
O2A—Dy1A—N1A	97.73 (16)	O2B—Dy1B—N1B	106.05 (15)
O2A—Dy1A—N2A	86.30 (15)	O2B—Dy1B—N2B	93.30 (16)
O2A—Dy1A—N5A	92.4 (2)	O2B—Dy1B—N4B	94.1 (2)
O2A—Dy1A—N3A	84.8 (4)	O2B—Dy1B—N5B	90.36 (17)
O2A—Dy1A—N4A	95.8 (4)	O2B—Dy1B—N3B	80.8 (3)
N1A—Dy1A—N2A	66.09 (19)	N1B—Dy1B—N2B	64.76 (19)
N1A—Dy1A—N5A	67.5 (2)	N1B—Dy1B—N4B	138.76 (19)
N1A—Dy1A—N3A	145.3 (2)	N1B—Dy1B—N5B	65.92 (19)
N1A—Dy1A—N4A	145.1 (2)	N1B—Dy1B—N3B	147.8 (2)
N5A—Dy1A—N2A	132.9 (2)	N4B—Dy1B—N2B	150.78 (19)
N5A—Dy1A—N3A	147.2 (2)	N4B—Dy1B—N3B	69.7 (2)

N5A—Dy1A—N4A	79.9 (2)	N5B—Dy1B—N2B	129.6 (2)
N3A—Dy1A—N2A	79.6 (2)	N5B—Dy1B—N4B	78.6 (2)
N4A—Dy1A—N2A	147.1 (2)	N5B—Dy1B—N3B	146.3 (2)
N4A—Dy1A—N3A	67.9 (3)	N3B—Dy1B—N2B	83.7 (2)

Table S4. Shape analysis for complex **1**. The lowest CShMs value, is highlighted. Continuous hape measures analysis estimates the distortion from the perfect polyhedron, where 0 corresponds to the ideal structure.[16]

	Dy1A	**Symmetry**	**Ideal polyhedron**
HP-7	31.955	D_{7h}	Heptagon
HPY-7	23.478	C_{6v}	Hexagonal pyramid
PBPY-7	**1.293**	$\boldsymbol{D_{5h}}$	**Pentagonal bipyramid**
COC-7	7.549	C_{3v}	Capped octahedron
CTPR-7	5.669	C_{2v}	Capped trigonal prism
JPBPY-7	2.308	D_{5h}	Johnson pentagonal bipyramid J13
JETPY-7	21.169	C_{3v}	Johnson elongated triangular pyramid J7
	Dy1B	**Symmetry**	**Ideal polyhedron**
HP-7	31.559	D_{7h}	Heptagon
HPY-7	22.873	C_{6v}	Hexagonal pyramid
PBPY-7	**1.681**	$\boldsymbol{D_{5h}}$	**Pentagonal bipyramid**
COC-7	5.453	C_{3v}	Capped octahedron
CTPR-7	3.935	C_{2v}	Capped trigonal prism
JPBPY-7	2.990	D_{5h}	Johnson pentagonal bipyramid J13
JETPY-7	21.169	C_{3v}	Johnson elongated triangular pyramid J7

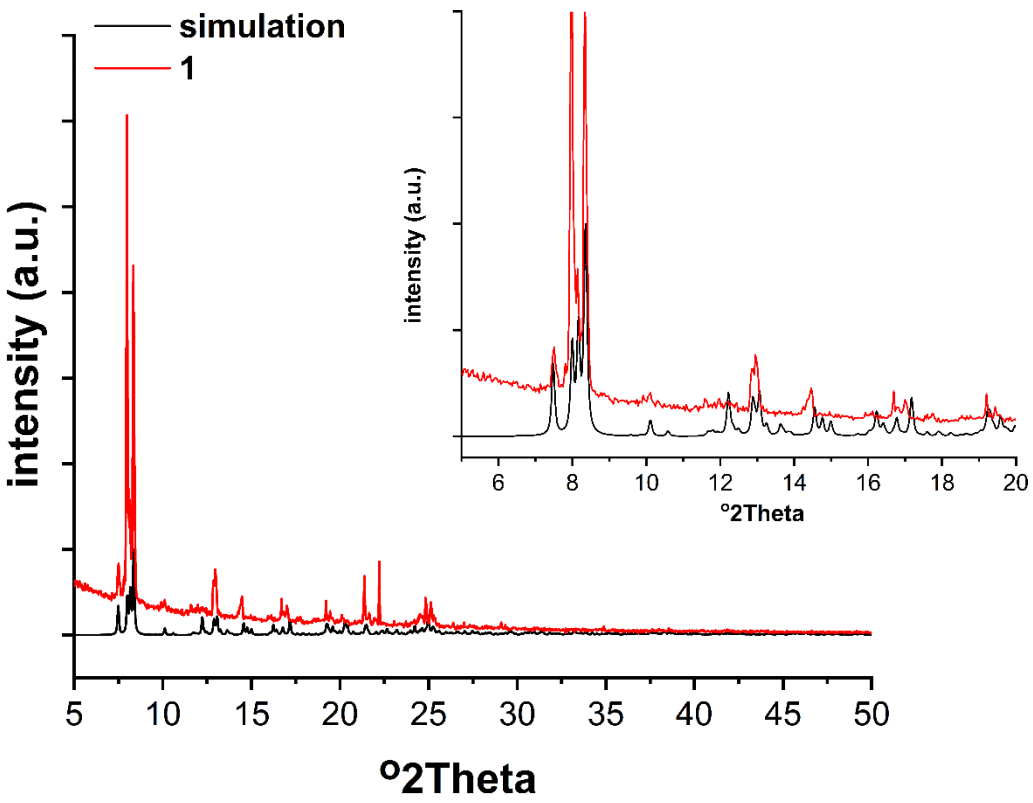

Fig. S1 The powder X-ray diffraction pattern of **1** (Inset: diffraction of **1** from 5-20°)**.** The black line represents the simulated powder X-ray diffraction pattern generated from single-crystal data collected at 150 K, and the red line represents the experimental data measured at ambient temperature.

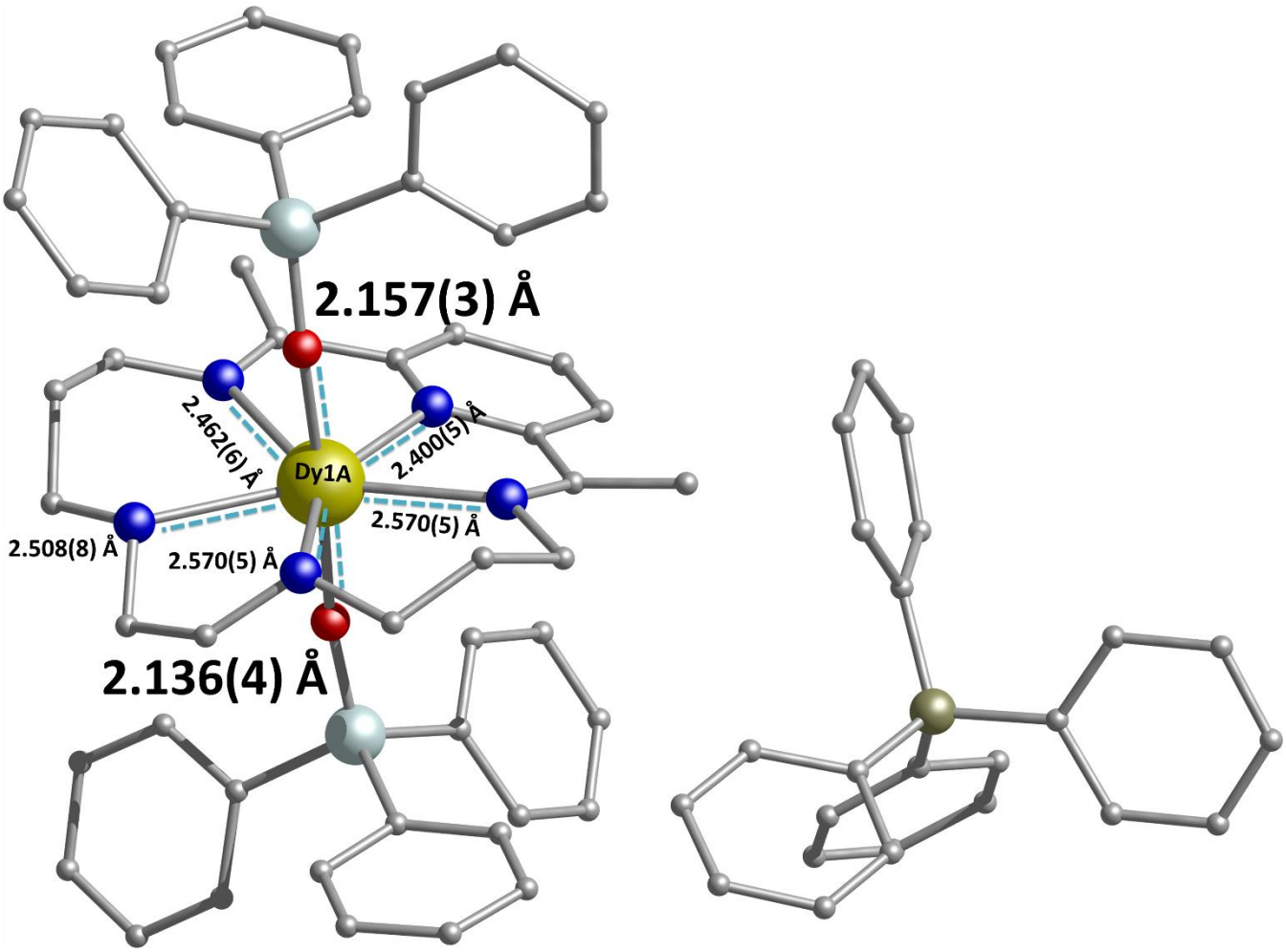

Fig. S2 Selected bond distances for complex **1** in Å emphasizing on the short O-Dy-O axial distances generated by the strong donor Ph_3SiO^- ligands and the longer Dy-N distances in the pentagonal plane generated by the L^{N5} ligand. Dy gold, O red, N blue, Si light turquoise, C gray, B dark yellow. Hydrogen atoms, disorder components and solvent molecules are omitted for clarity.

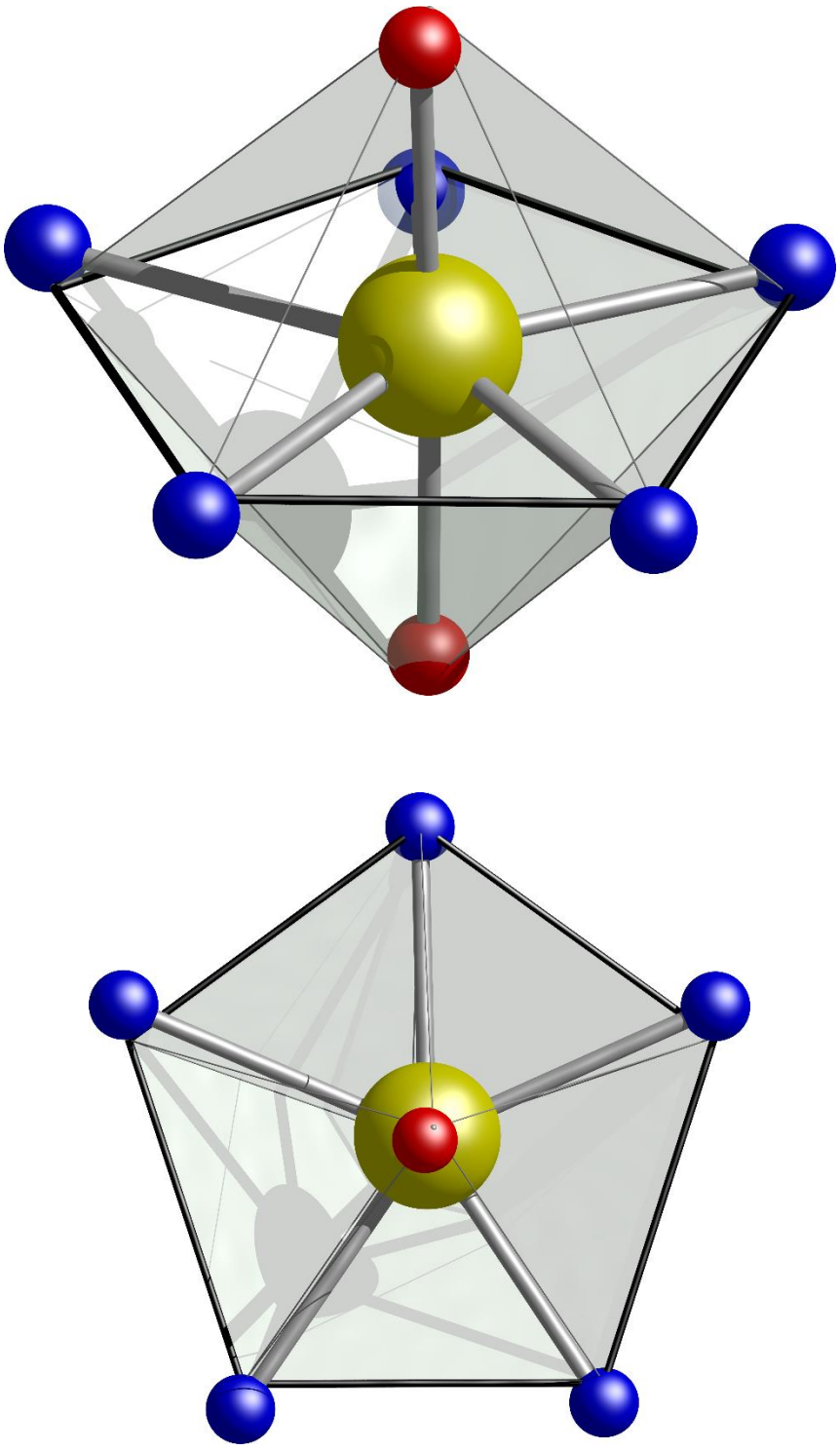

Fig. S3 (upper) Comparison of the calculated (with SHAPE)[16] and experimental compressed pentagonal bipyramidal coordination sphere for the Dy(III) ion in **1**. (Lower) The highlighted pentagonal bipyramidal plane of the polydentate ligand $\mathbf{L^{N5}}$ ligand. Dy, gold; N, dark blue; O, red.

3. Magnetic Properties

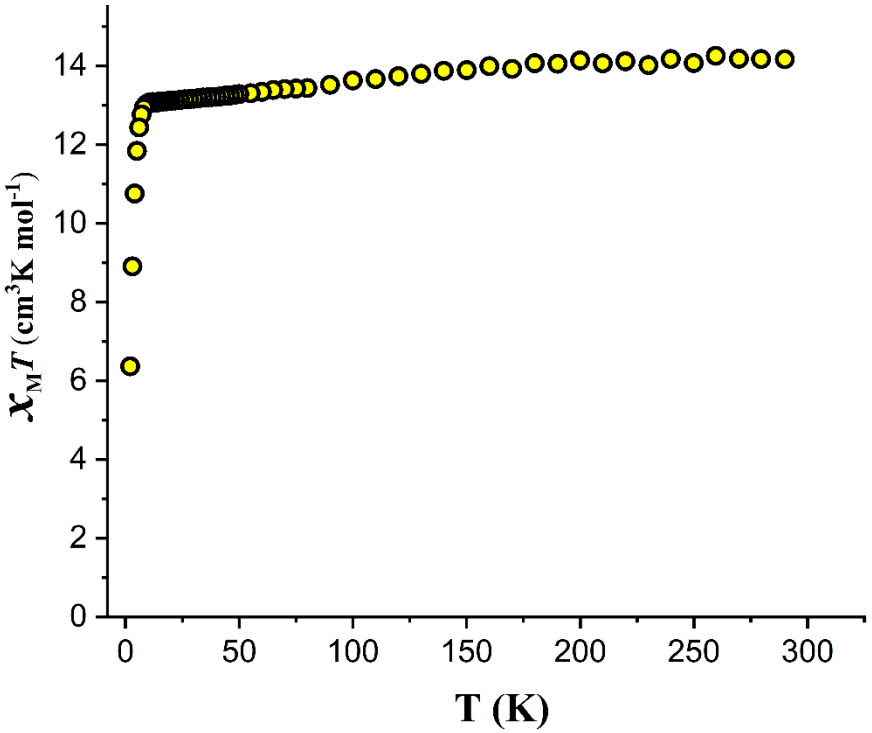

Fig. S4 $\chi_M T$ vs. T data for **1** in a field of 1000 Oe from 290 – 2 K.

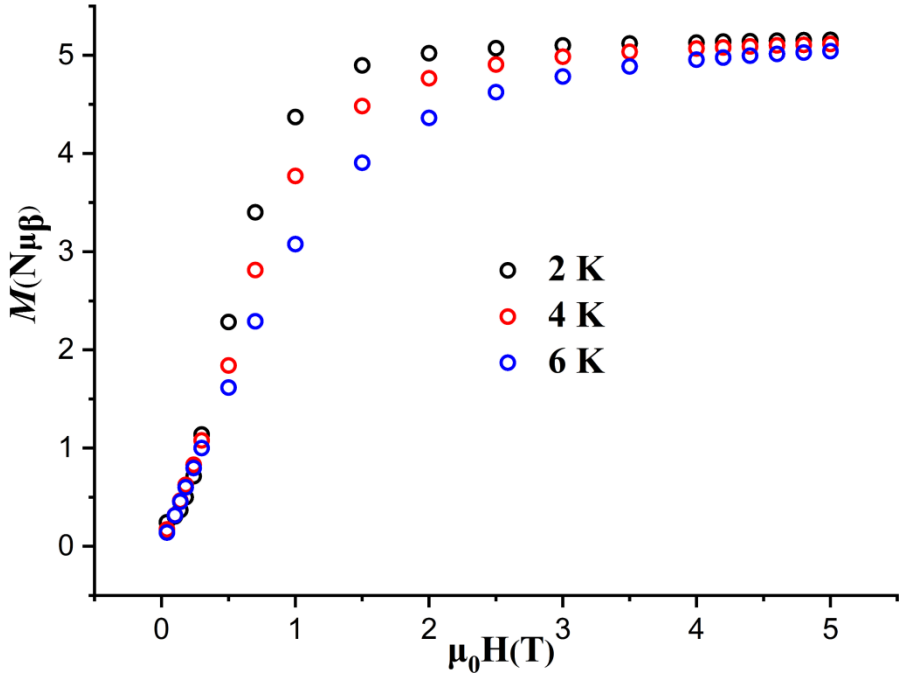

Fig. S5 Magnetisation vs. Field plot at temperatures 2, 4 and 6 K for **1** from 0.04-5 T.

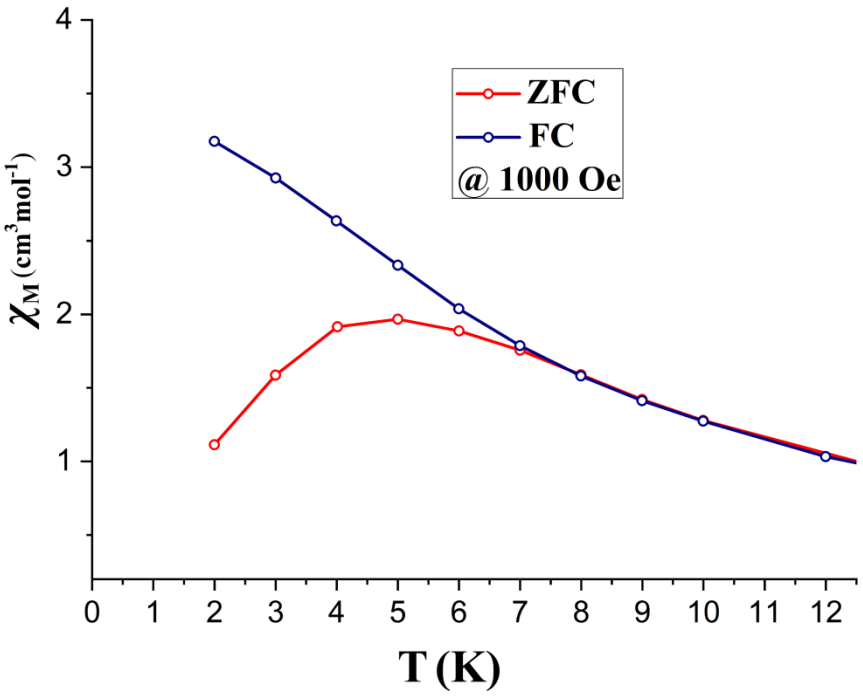

Fig. S6 The Field cooled (FC) and Zero-Field cooled (ZFC) magnetic susceptibility of **1** at 1000 Oe diverging at 7 K with the maximum observed at ~ 5 K.

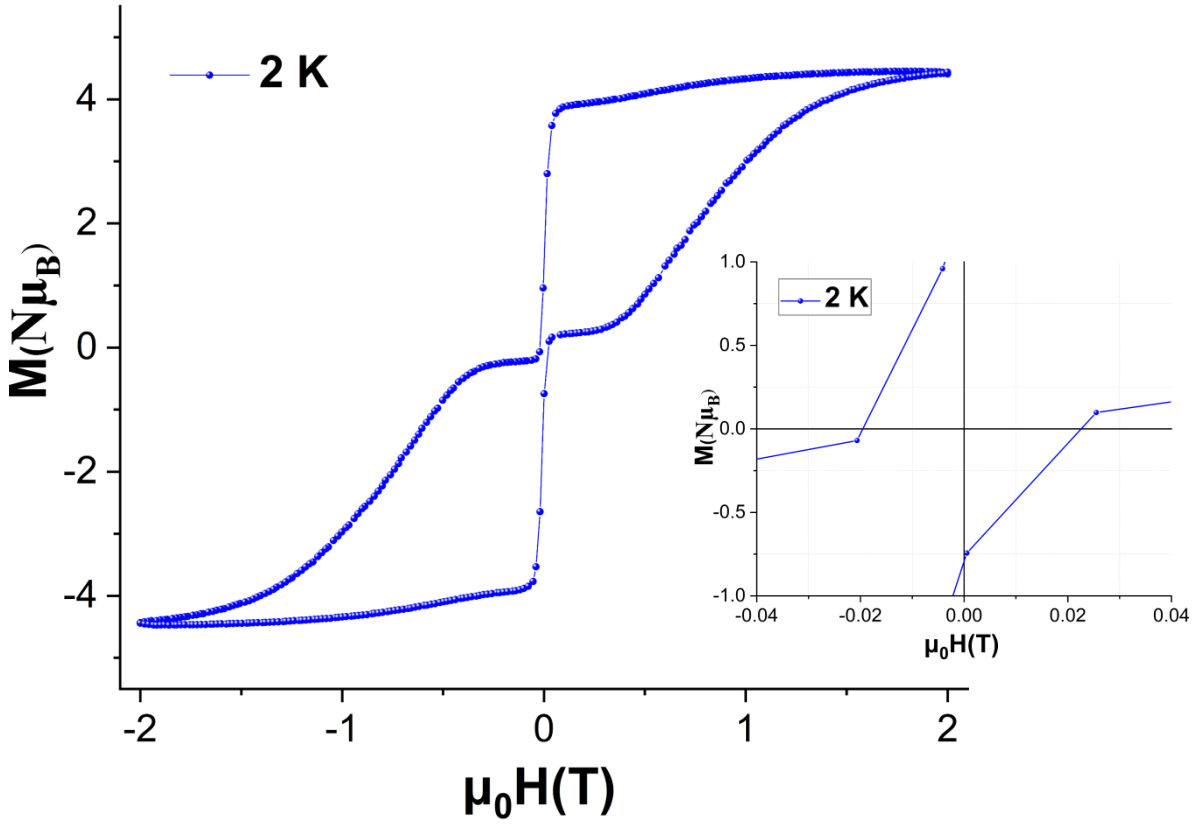

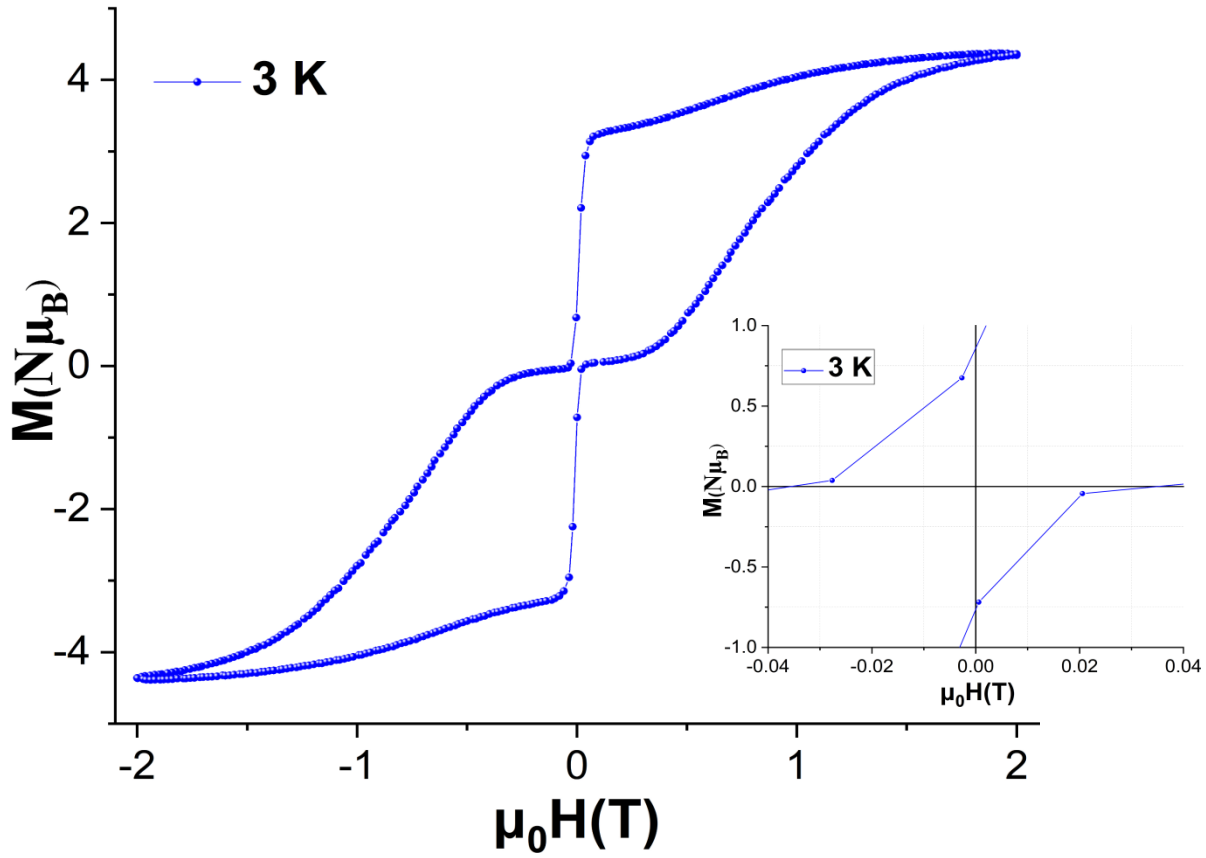
3 K
M(Nμ_B)
μ_0H(T)
4
2
0
-2
-4
-2
-1
0
1
2
3 K
1.0
0.5
0.0
-0.5
-1.0
-0.04
-0.02
0.00
0.02
0.04
μ_0H(T)

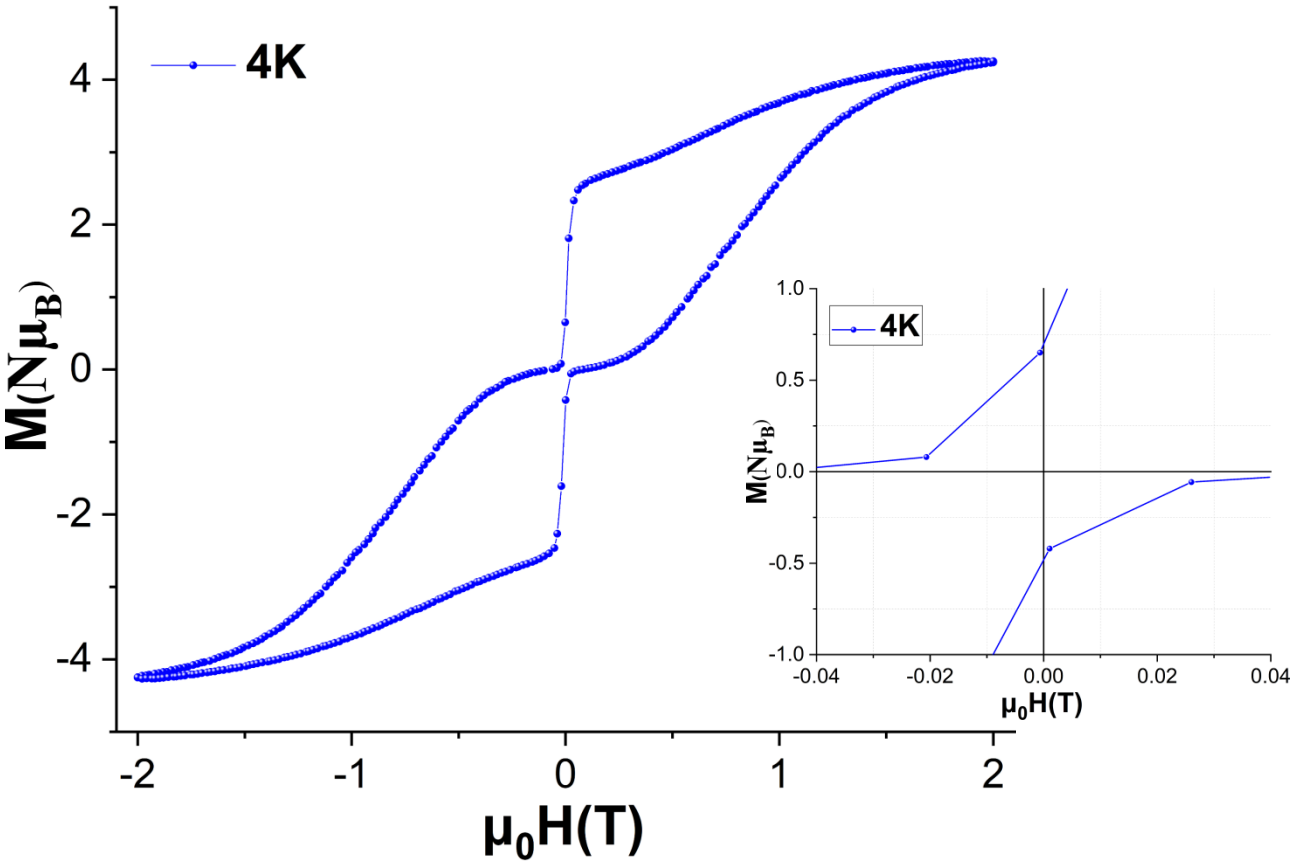
4K
M(Nμ_B)
μ_0H(T)
4
2
0
-2
-4
-2
-1
0
1
2
4K
1.0
0.5
0.0
-0.5
-1.0
-0.04
-0.02
0.00
0.02
0.04
μ_0H(T)

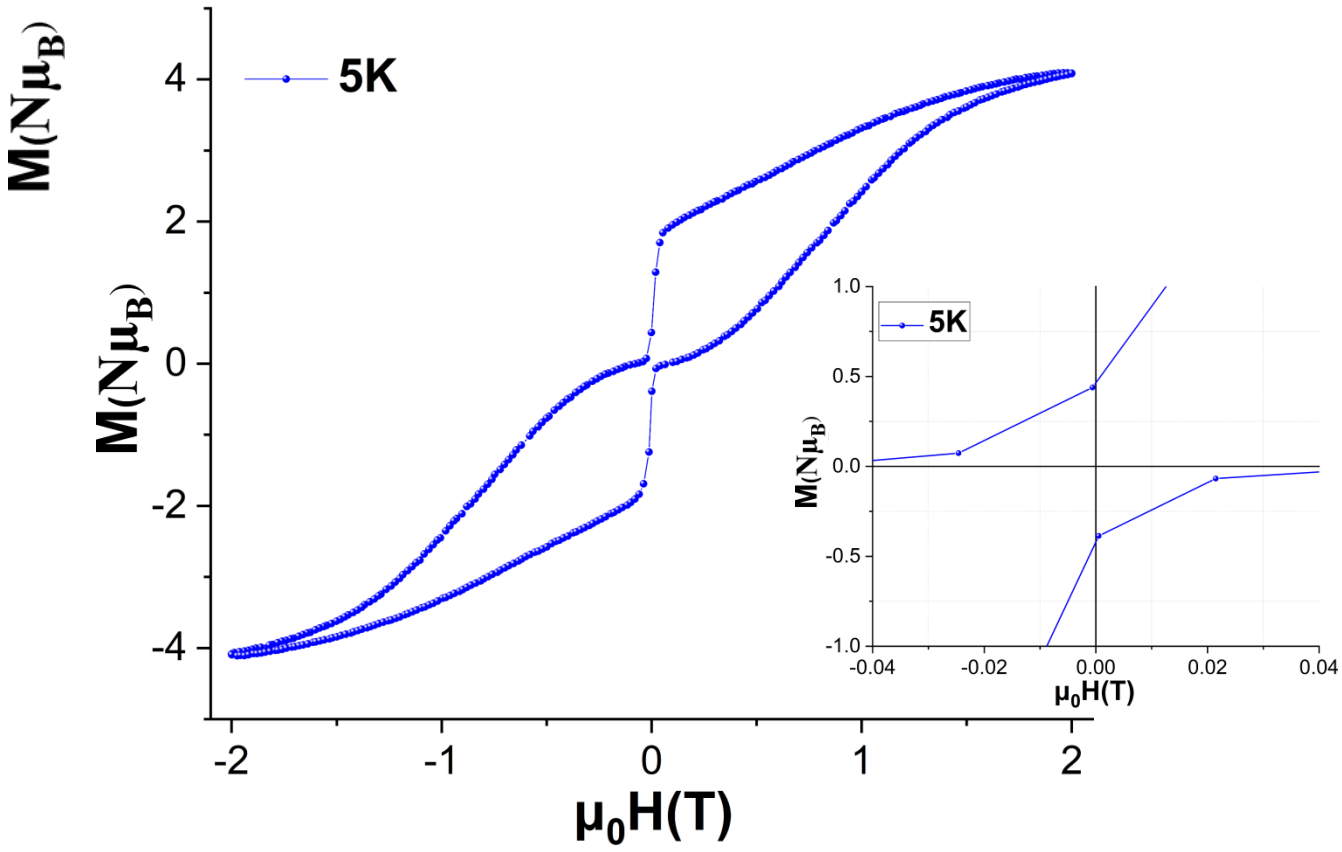
5K
M(Nμ_B)
μ_0H(T)
4
2
0
-2
-4
-2
-1
0
1
2
5K
1.0
0.5
0.0
-0.5
-1.0
-0.04
-0.02
0.00
0.02
0.04
M(Nμ_B)
μ_0H(T)

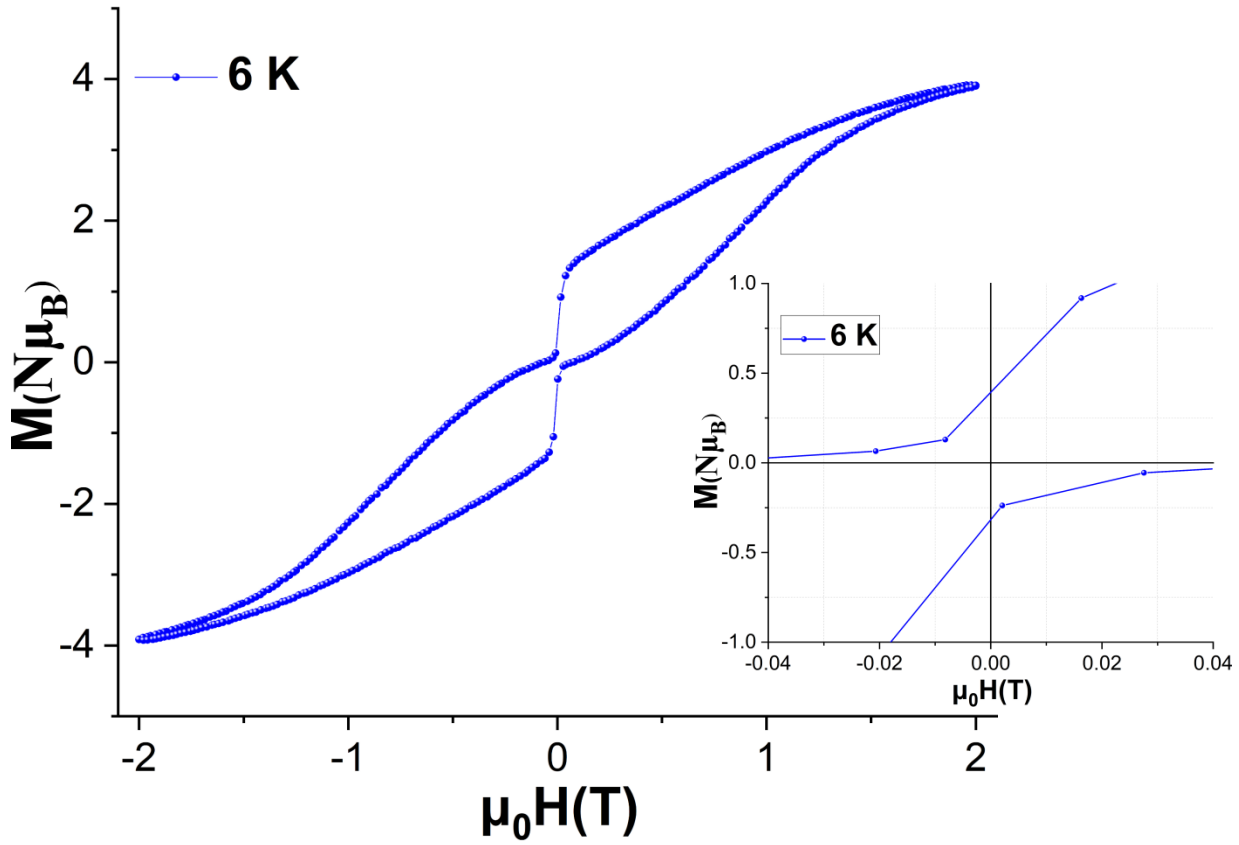
6 K
M(Nμ_B)
μ_0H(T)
4
2
0
-2
-4
-2
-1
0
1
2
6 K
1.0
0.5
0.0
-0.5
-1.0
-0.04
-0.02
0.00
0.02
0.04
M(Nμ_B)
μ_0H(T)

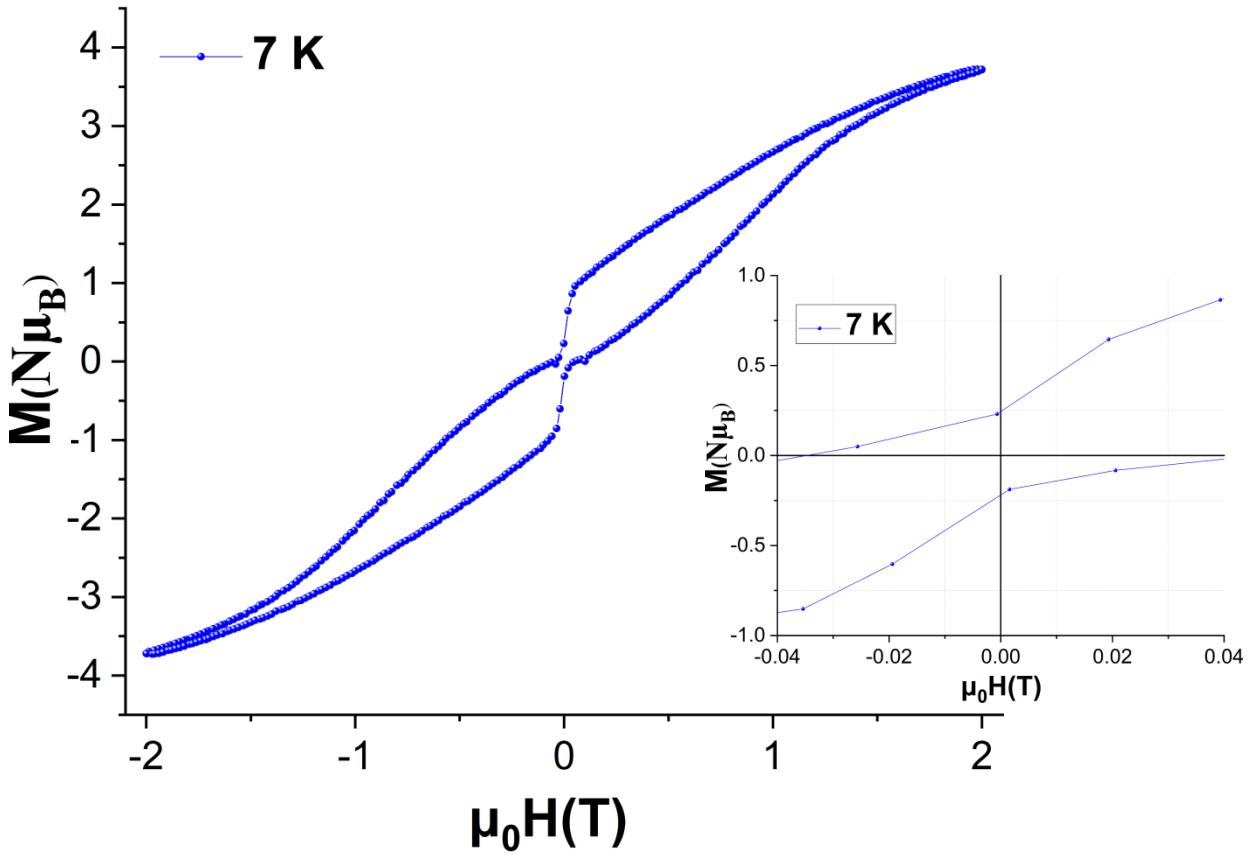
7 K
M(Nμ_B)
μ_0H(T)
7 K
M(Nμ_B)
μ_0H(T)

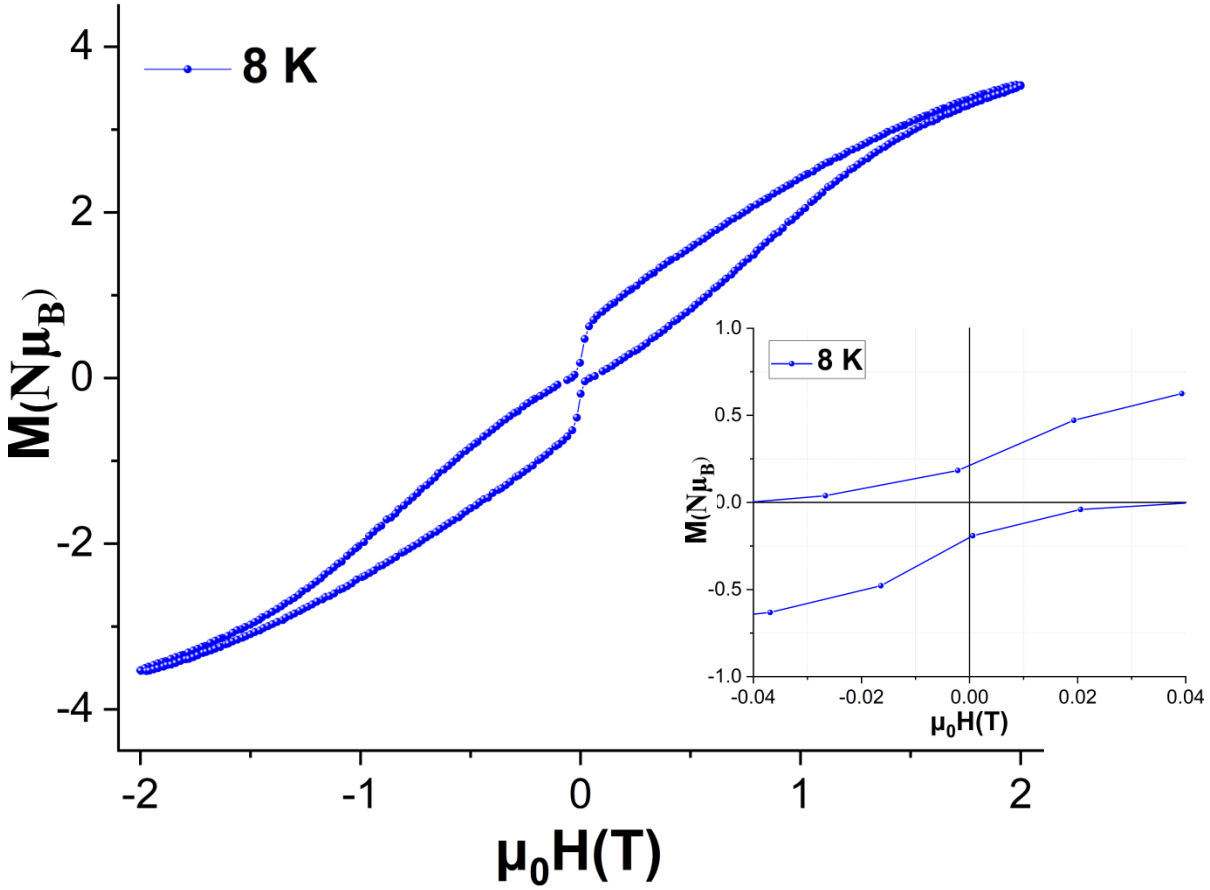
8 K
M(Nμ_B)
μ_0H(T)
8 K
M(Nμ_B)
μ_0H(T)

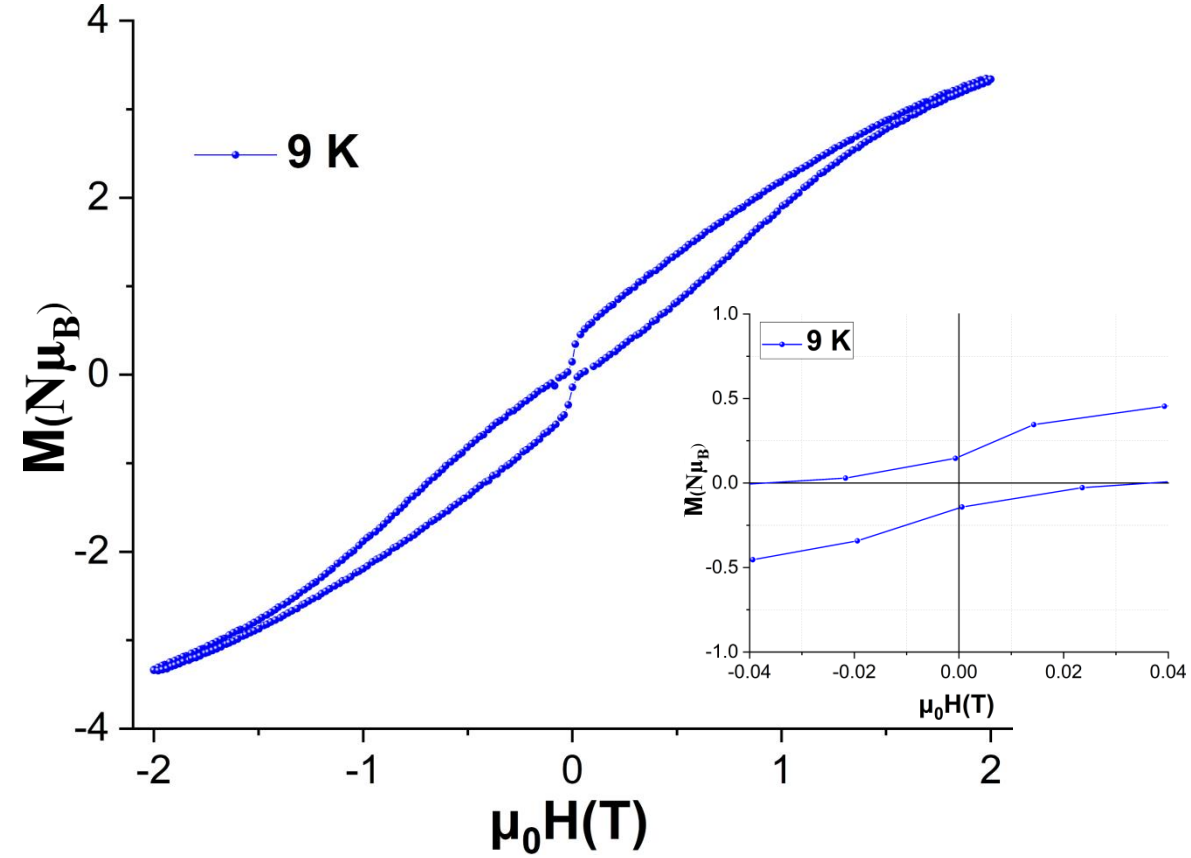
9 K
M(Nμ_B)
μ_0H(T)
9 K
M(Nμ_B)
μ_0H(T)

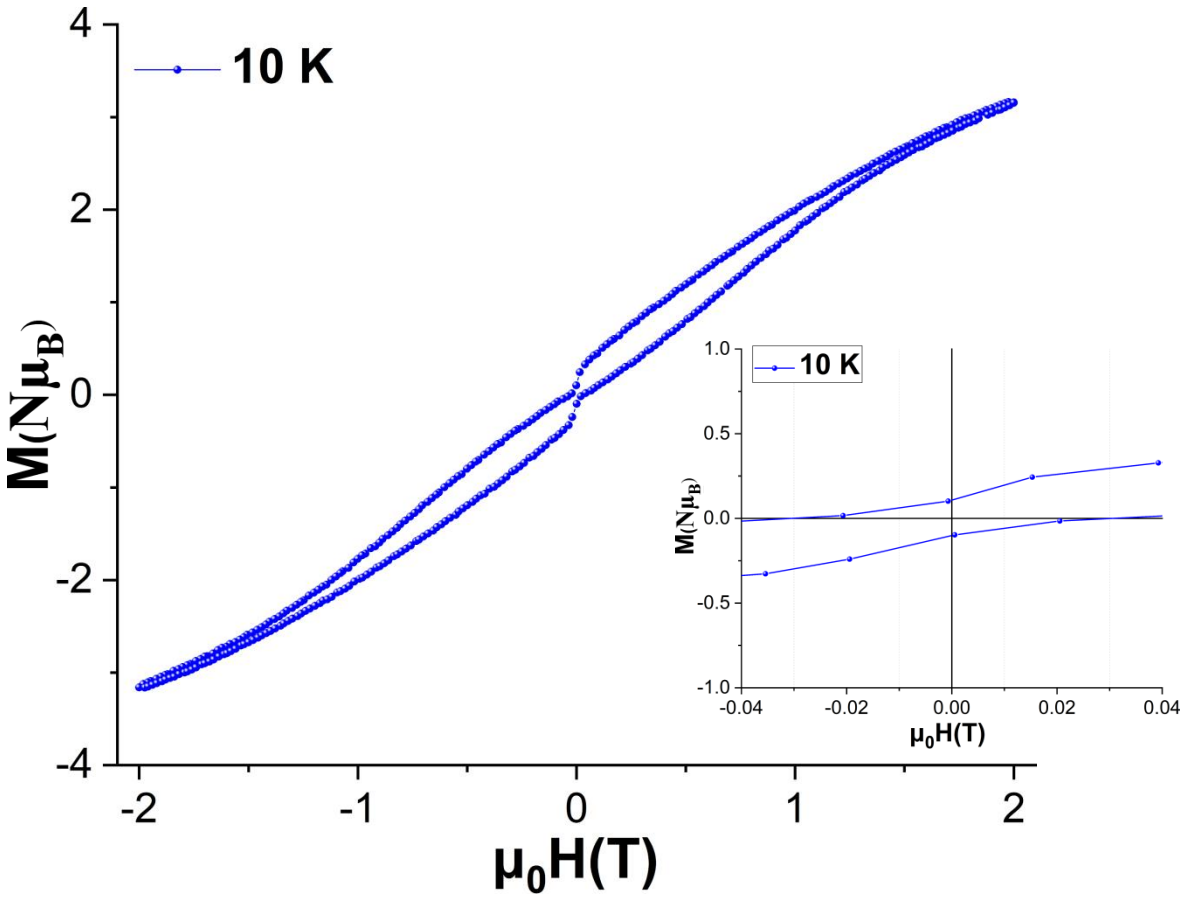
10 K
M(Nμ_B)
μ_0H(T)
10 K
M(Nμ_B)
μ_0H(T)

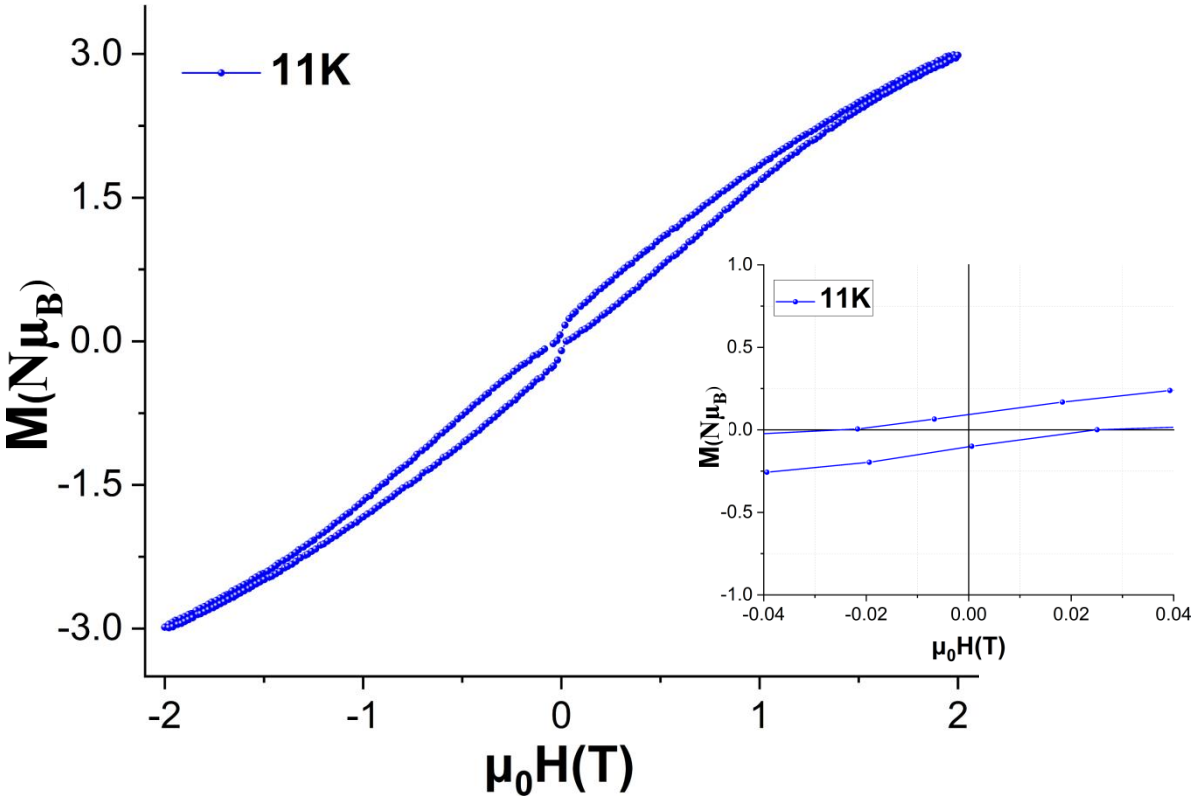
11K
M(Nμ_B)
μ_0H(T)
3.0
1.5
0.0
-1.5
-3.0
-2
-1
0
1
2
11K
M(Nμ_B)
μ_0H(T)
1.0
0.5
0.0
-0.5
-1.0
-0.04
-0.02
0.00
0.02
0.04

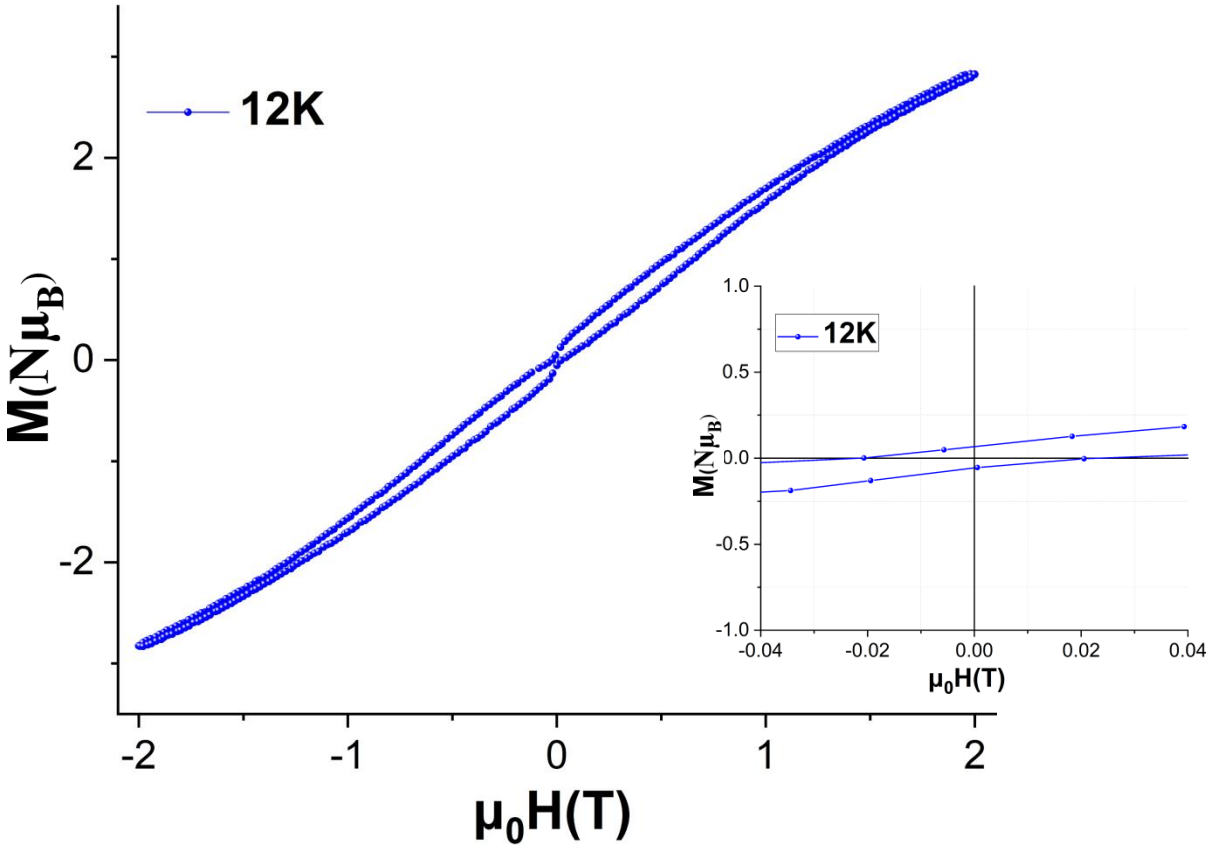
12K
M(Nμ_B)
μ_0H(T)
2
0
-2
-2
-1
0
1
2
12K
M(Nμ_B)
μ_0H(T)
1.0
0.5
0.0
-0.5
-1.0
-0.04
-0.02
0.00
0.02
0.04

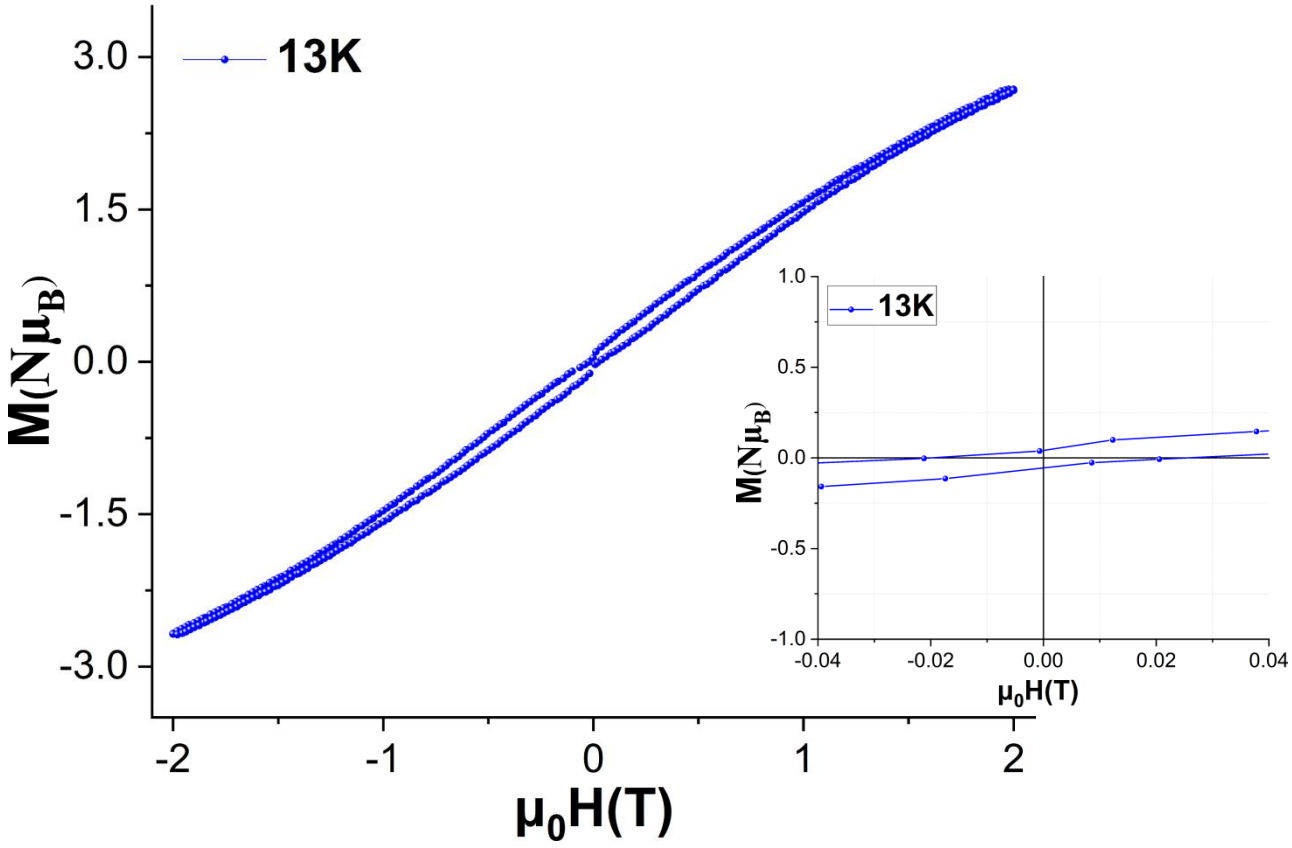
13K
M(Nμ_B)
μ_0H(T)
3.0
1.5
0.0
-1.5
-3.0
-2
-1
0
1
2
13K
1.0
0.5
0.0
-0.5
-1.0
-0.04
-0.02
0.00
0.02
0.04

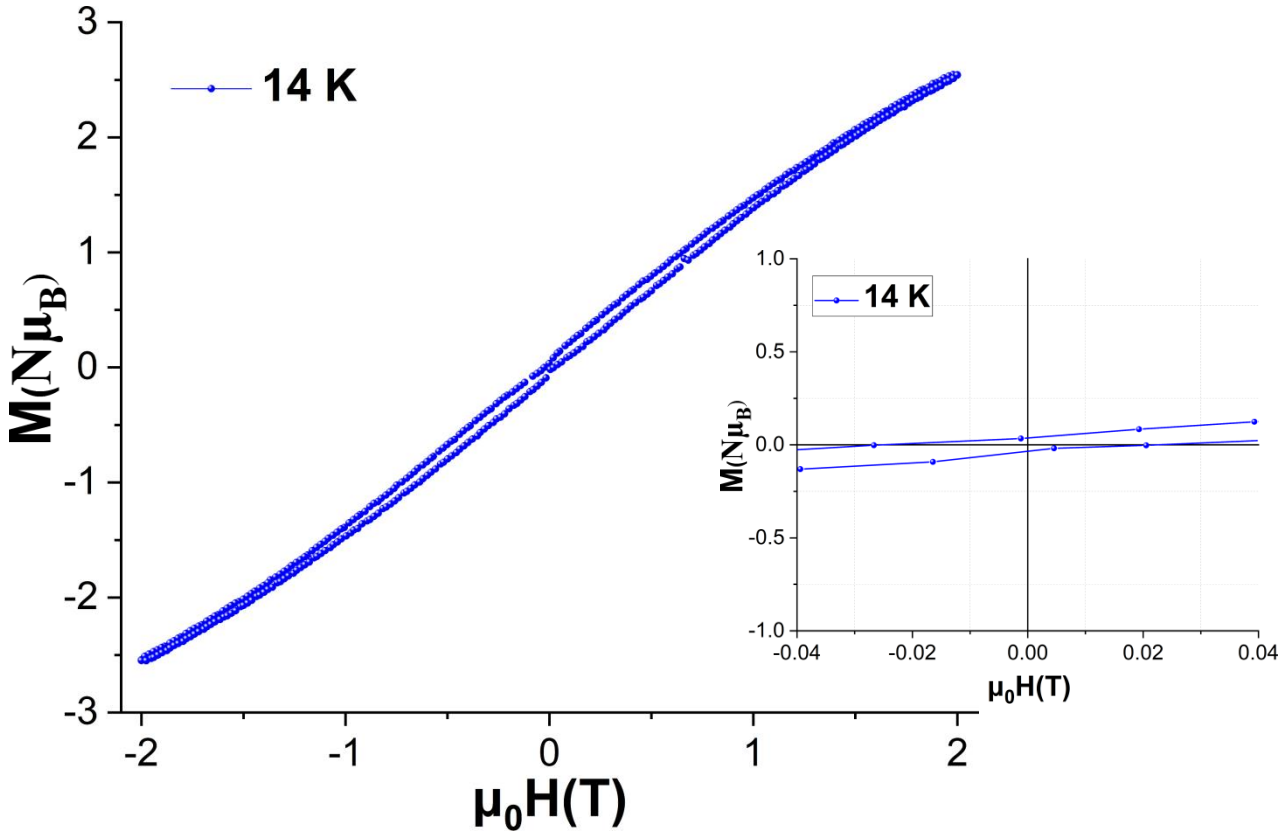
14 K
M(Nμ_B)
μ_0H(T)
3
2
1
0
-1
-2
-3
-2
-1
0
1
2
14 K
1.0
0.5
0.0
-0.5
-1.0
-0.04
-0.02
0.00
0.02
0.04

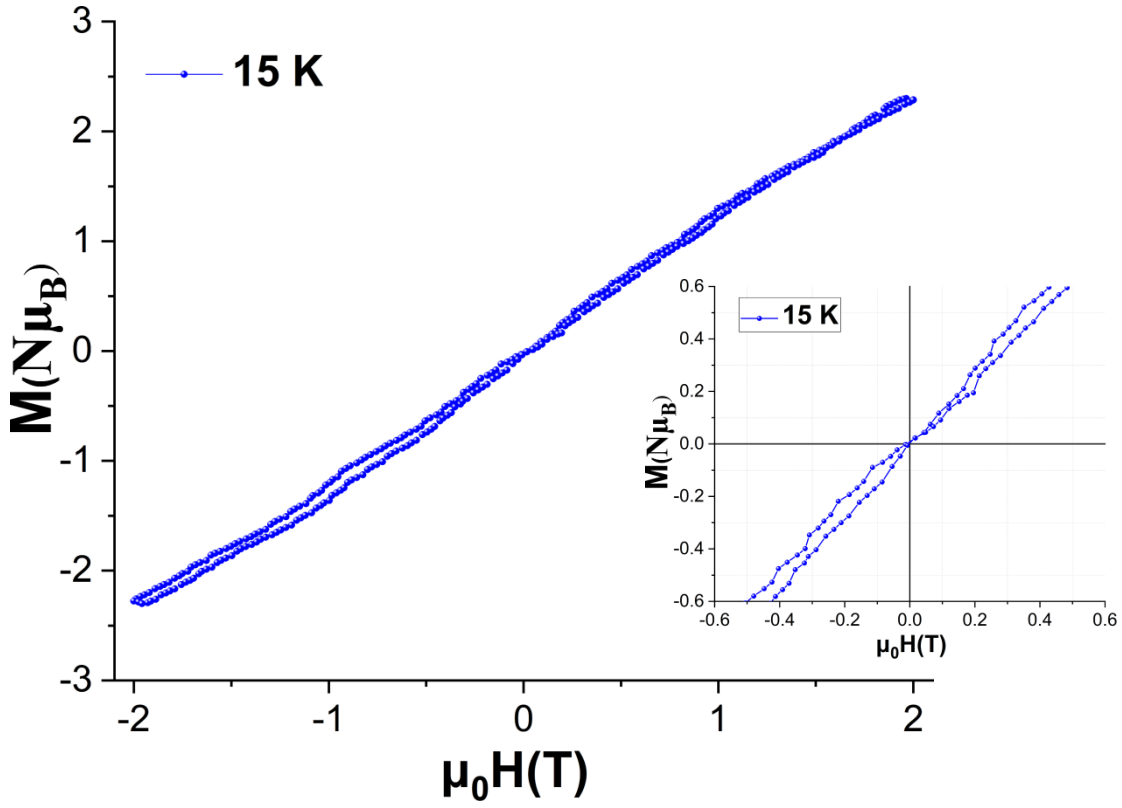

Fig. S7 Powder magnetic hysteresis measurements for **1** at 2-15 K with an average sweep rate of 0.01 Ts^{-1}.

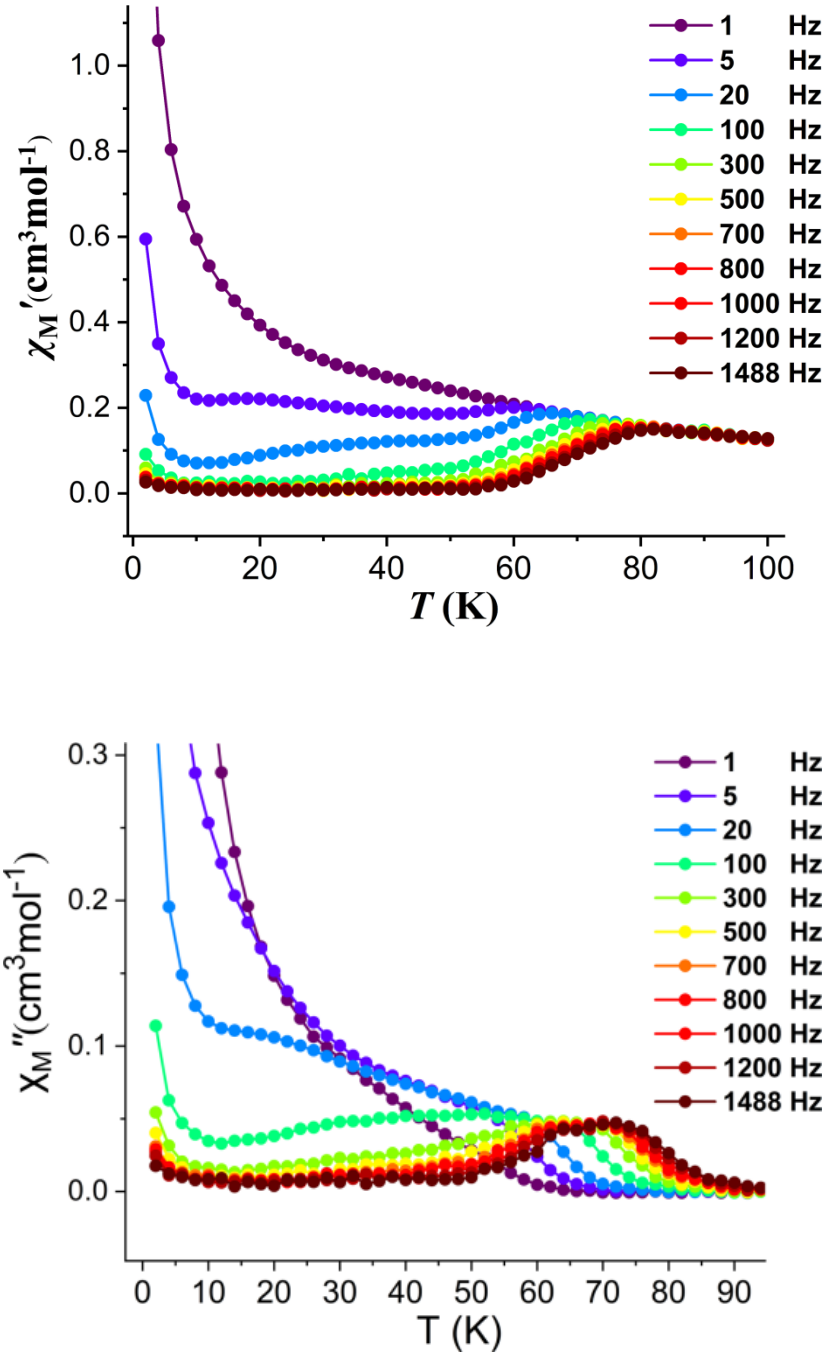

Fig. S8 Temperature dependence of the in-phase, χ'_M (upper) and out-of-phase, χ''_M (lower) ac susceptibility, in zero dc field, for **1** with ac frequencies of 1–1488 Hz.

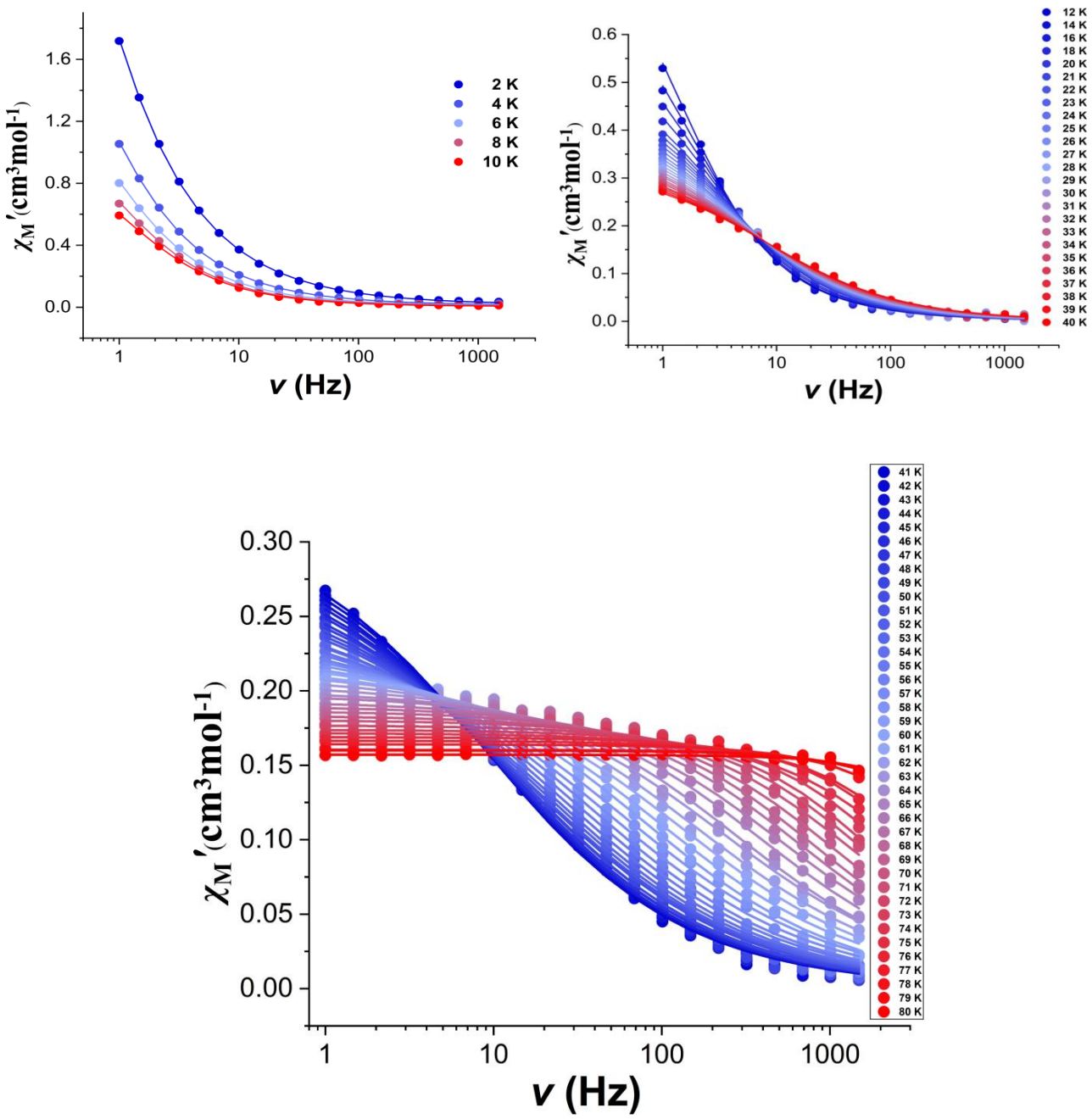

Fig. S9 Frequency dependence of the in phase ac susceptibility for **1** up to 80 K in zero dc field. The solid lines correspond to the best fit to Debyes's law.[17]

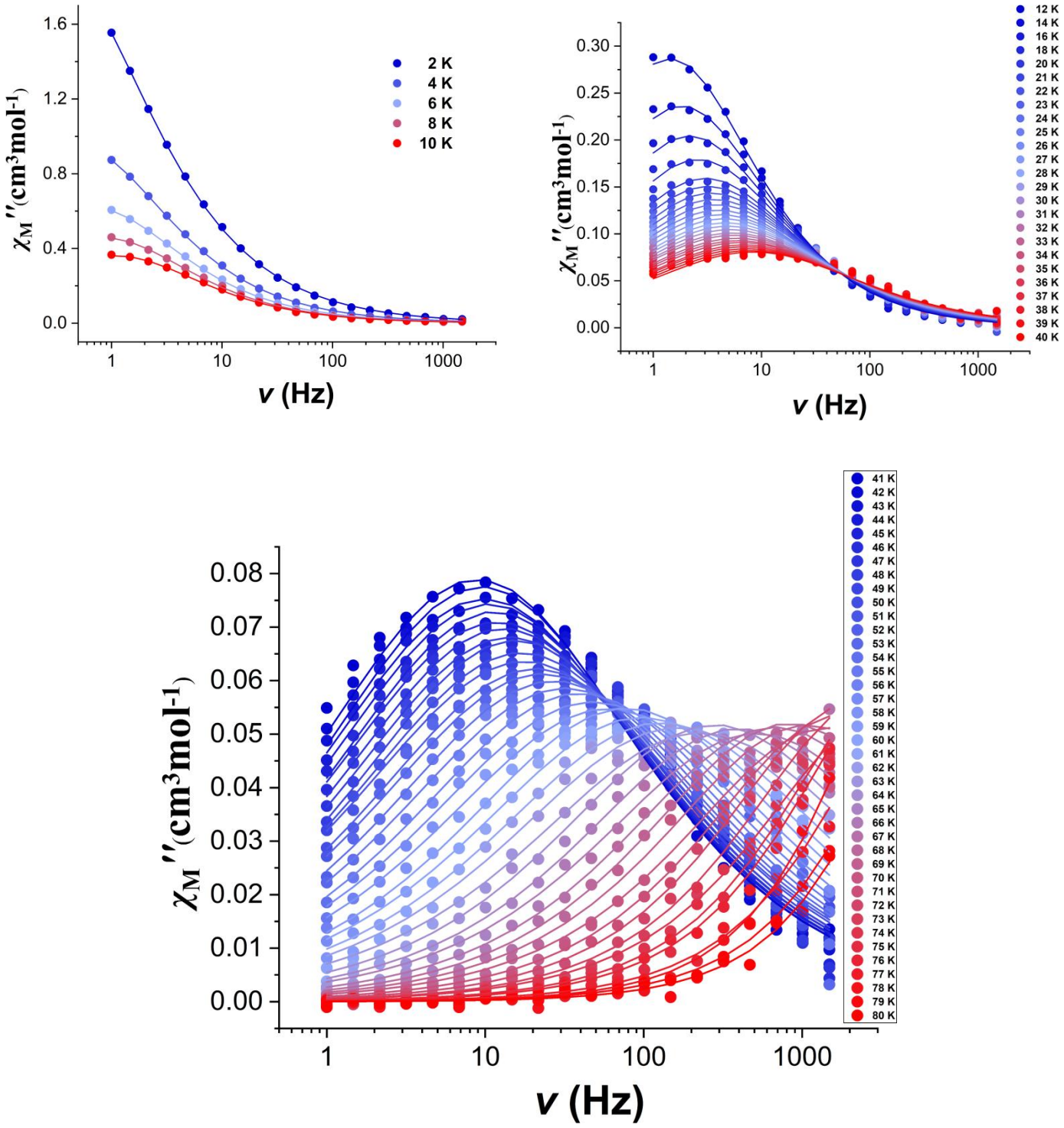

Fig. S10 Frequency dependence of the out-of- phase ac susceptibility for **1** up to 80 K in zero dc field. The solid lines correspond to the best fit to Debyes's law.[17]

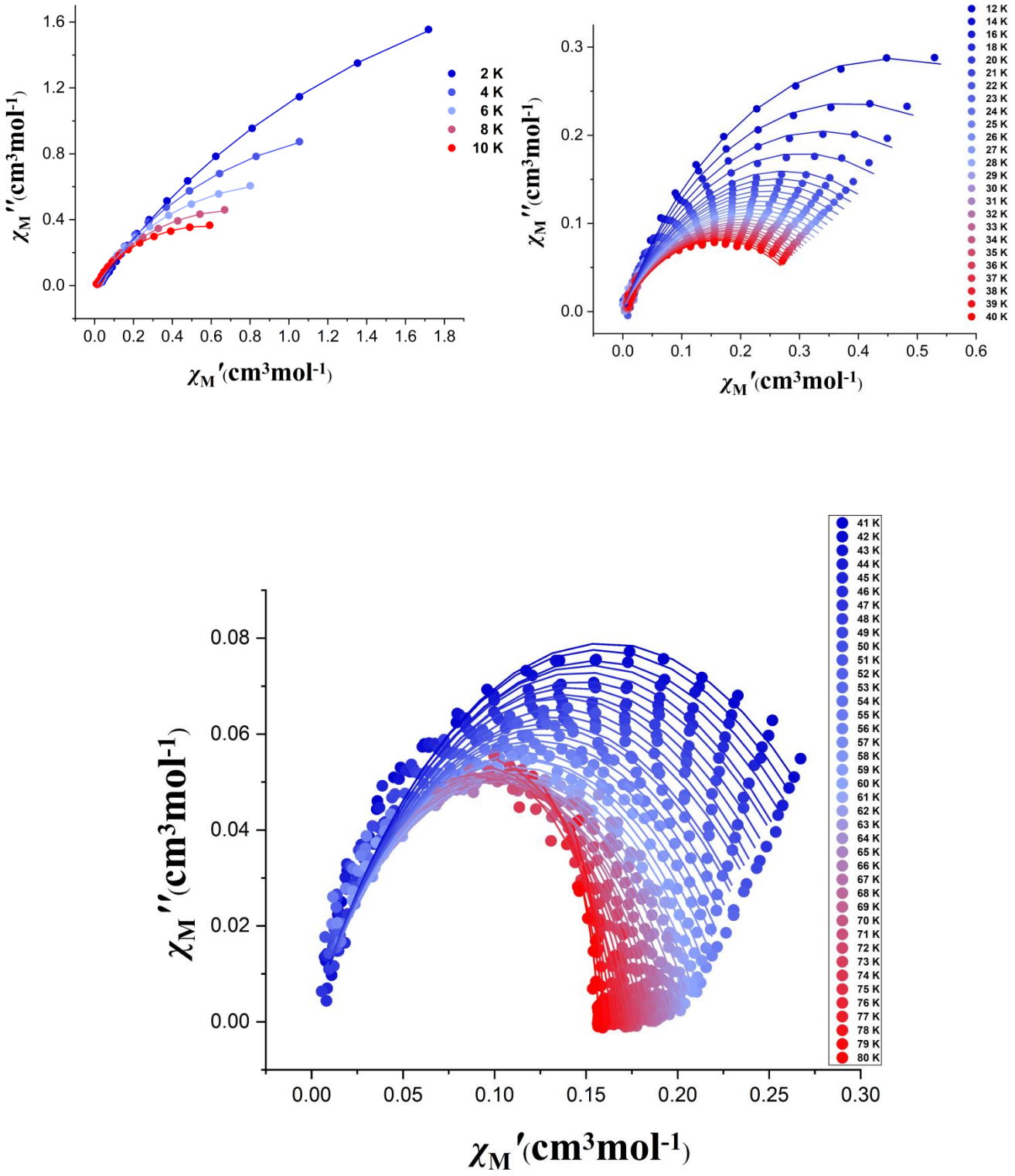

Fig. S11 χ''_M vs χ'_M plot of the AC magnetic susceptibility of **1** in zero dc field. The solid lines correspond to the best fit to Debye's law.[17]

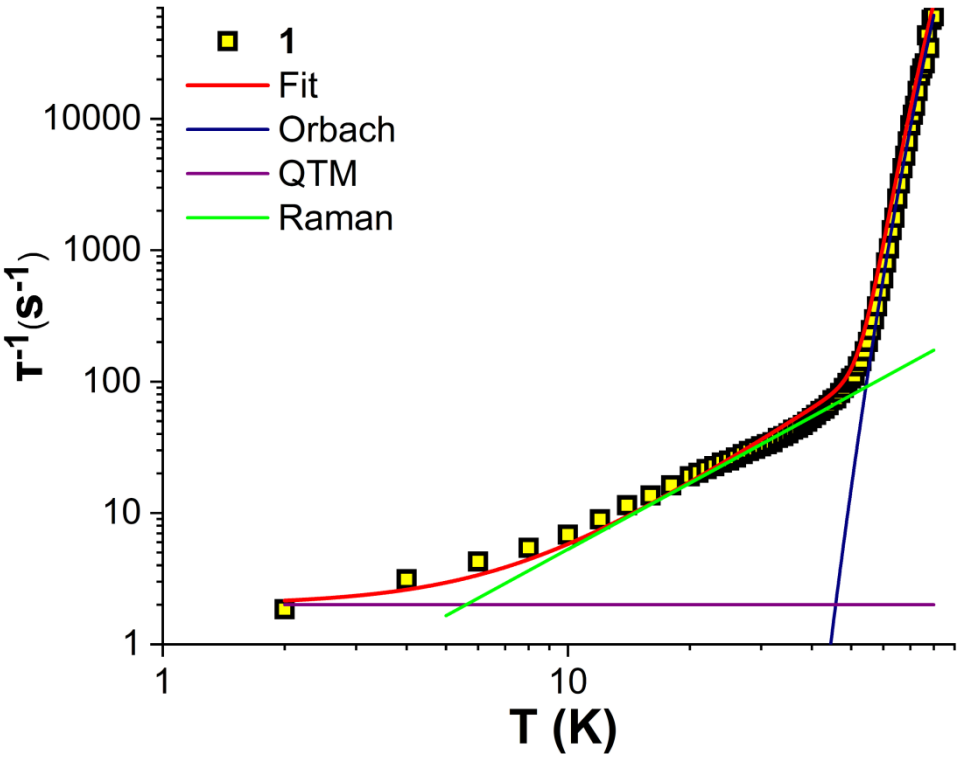

Fig. S12 Log-Log plot of the relaxation times, τ^{-1} versus T for **1**. The data were analysed using the equation: $\tau^{-1} = \tau_{QTM}^{-1} + CT^{n} + \tau_{0}^{-1} \exp(-U_{eff}/T)$. The best fit (red line) gives n = 2.05, C = 3.0 10^{-2} K^{-n} s^{-1}, τ_{QTM} = 0.5 s , τ_0 = 1.56 x 10^{-11} s and U_{eff} = 1108 K.

4. Ab initio calculations

Computational Details:

All the *ab initio* CASSCF/RASSI-SO/SINGLE_ANISO calculations have been performed on the crystallographically independent molecules of **1** (including the counter ions and solvent molecules) using MOLCAS 8.2 programme package.[18] The basis set for our calculation has been taken from the ANO-RCC library implemented in the above package. We have used the following basis set; [Dy.ANO-RCC...7s6p4d2f1g.], [Cl.ANO-RCC...5s4p2d1f.], [P.ANO-RCC...4s3p.], [N.ANO-RCC...4s3p2d1f.], [O.ANO-RCC...4s3p2d1f.], [Si.ANO-RCC...4s3p.], [B.ANO-RCC...3s2p1d.], [C.ANO-RCC...3s2p.], [H.ANO-RCC...2s.] in our calculation. The Cholesky decomposition technique was used to reduce the computational cost. The spin orbit interaction has been included by DKH Hamiltonian. The spin free wave functions have been generated with CAS(9,7) active space which considers nine electrons in seven 5f orbitals. We have used only 21 sextets in our calculation since it has been found to reproduce the experimental observables.[10, 19] The spin orbit interaction has been included with RASSI-SO which mixes the spin free wave functions. Finally the g tensor, magnetic susceptibility etc. has been computed with SINGLE_ANISO.

The model system **1-N3O2** is created by replacing the -NH- groups of the L^{N5} ligand of Dy1A with oxygen groups. The model **1-O5** has been created by replacing the equatorial backbone of Dy1A with 16-crown-5.[20] The model then was optimized (replacing the Dy(III) ion with Gd(III) to avoid spin orbit coupling with the DFT framework) using the UB3LYP functional[21] in Gaussian09[22] programme package. We have used CSDZ[23] (Cundari Stevens Double Zeta) ECP with its corresponding basis set for Gd, Ahlrichs triple-ξ (TZV)[24] basis set for Si and O, split valence basis set (SVP) for C and H in the optimization process.

Table S5. CASSCF+RASSI-SO computed relative energies (in K) of the eight low lying Kramers Doublets (KDs) along with *g* tensors and deviations from the principal magnetisation axis with respect to the first KD for complex **1**.

Dy1A					
E (K)	**g_{xx}**	**g_{yy}**	**g_{zz}**	**Angle (°)**	**Composition of m_J levels**
0	0.001	0.001	19.979		1.00|±15/2>
602.1	0.046	0.058	17.040	3.7	0.99|±13/2>
1032.9	1.156	5.135	10.805	12.3	0.70|±11/2>+0.15|±1/2>+10|±3/2>
1102.6	0.529	3.350	13.758	92.2	0.53|±1/2>+0.21|±11/2>+0.17|±3/2>
1195.2	2.535	2.771	13.417	95.6	0.37|±3/2>+0.22|±5/2>+0.16|±7/2>
1311.9	3.284	5.541	10.543	74.0	0.48|±9/2>+0.20|±5/2>+0.10|±7/2>
1379.8	0.685	1.777	17.217	106.1	0.29|±5/2>+0.29|±7/2>+0.14|±9/2>

1527.3	0.169	0.404	18.690	64.9	0.43|±7/2>+0.20|±9/2>+0.22|±5/2>

Dy1B					
E (K)	**g_{xx}**	**g_{yy}**	**g_{zz}**	**Angle (°)**	**Composition of m_J levels**
0	0.000	0.000	19.984		1.00|±15/2>
606.9	0.055	0.063	17.009	2.8	0.99|±13/2>
1051.9	1.152	3.247	12.114	26.7	0.77|±11/2>+0.12|±1/2>
1160.7	1.384	2.352	13.732	77.2	0.48|±1/2>+0.22|±3/2>0.08|±5/2>
1277.4	0.825	2.132	15.483	80.8	0.37|±3/2>+0.20|±5/2>+0.12|±7/2>
1363.7	7.708	6.699	4.570	77.9	0.52|±9/2>+0.19|±3/2>+0.08|±1/2>
1425.8	0.151	1.700	15.222	66.5	0.35|±7/2>+0.34|±5/2>+0.19|±9/2>
1529.1	0.771	1.947	17.400	67.9	0.45|±7/2>+0.24|±5/2>+0.11|±9/2>

Table S6. CASSCF+RASSI-SO computed relative energies of the eight low lying Kramers Doublets (KDs) along with g tensors and deviations from the principal magnetisation axis with respect to the first KD for model **1-N3O2**.

Model 1-N3O2 (changing equatorial ligand)					
E (K)	**g_{xx}**	**g_{yy}**	**g_{zz}**	**Angle (°)**	**Composition of m_J levels**
0.0	0.000	0.000	19.981		1.00|±15/2>
658.1	0.028	0.032	17.046	0.5	1.00|±13/2>
1190.5	0.453	0.672	13.985	6.4	0.95|±11/2>
1438.1	0.769	2.647	15.608	88.8	0.62|±1/2>+0.22|±3/2>
1497.0	0.985	5.035	10.540	107.9	0.36|±9/2>+0.24|±3/2>+0.16|±5/2>
1581.9	0.922	4.261	8.189	112.3	0.37|±9/2>+0.24|±3/2>+0.17|±5/2>
1646.0	2.330	5.328	12.990	92.3	0.34|±5/2>+0.19|±3/2>+0.17|±1/2>
1795.1	0.666	0.996	18.016	66.6	0.47|±7/2>+0.30|±5/2>

Table S7. CASSCF+RASSI-SO computed relative energies of the eight low lying Kramers Doublets (KDs) along with g tensors and deviations from the principal magnetisation axis with respect to the first KD for model **1-O5**.

Model 1-O5 (changing equatorial ligand)					
E (K)	**g_{xx}**	**g_{yy}**	**g_{zz}**	**Angle (°)**	**Composition of m_J levels**
0.0	0.000	0.000	19.990		1.00|±15/2>
758.1	0.014	0.015	17.014	0.1	1.00|±13/2>
1377.6	0.198	0.209	14.163	2.8	0.99|±11/2>
1788.6	1.465	1.542	10.818	6.2	0.92|±9/2>+0.04|±3/2>
1931.0	0.456	1.809	17.717	89.1	0.73|±1/2>+0.21|±3/2>
1965.3	8.990	7.340	4.300	17.4	0.65|±7/2>+0.26|±5/2>
1993.6	0.198	1.829	14.339	86.4	0.57|±3/2>+0.28|±5/2>+0.05|±7/2>
2114.3	0.074	1.361	18.003	82.5	0.42|±5/2>+0.27|±7/2>+0.17|±3/2>

Table S8. The *ab initio* computed crystal field parameters for complex **1** and for model systems **1-N3O2** and **1-O5**.

k	**q**	**B_k^q (1DyA)**	**B_k^q (1-DyB)**	**B_k^q (1-N3O2)**	**B_k^q (1-O5)**
2	-2 -1 **0** 1 2	-1.70E+00 -9.47E-01 **-4.96E+00** 1.78E+00 5.67E-01	7.53E-01 5.49E-01 **-5.20E+00** 1.32E+00 -1.52E+00	-1.04E+00 -8.63E-01 **-6.29E+00** 1.86E+00 5.62E-01	-4.13E-02 8.54E-01 **-8.17E+00** -2.10E-01 -6.11E-01
$\lvert B_2^0 \rvert / \lvert$ av. non-axial $\rvert$		3.97	5.02	5.82	19.0

4	-4 -3 -2 -1 **0** 1 2 3 4	1.41E-03 1.18E-02 8.18E-03 4.85E-03 **-1.47E-02** -7.63E-03 -1.09E-04 -1.10E-02 -1.35E-02	-8.17E-03 -1.17E-02 6.62E-04 -6.55E-03 **-1.42E-02** -5.99E-03 4.84E-03 8.84E-03 -2.52E-03	2.33E-03 6.75E-03 6.94E-03 6.00E-03 **-1.42E-02** -9.32E-03 7.75E-05 -1.46E-02 -1.12E-02	2.49E-03 2.41E-03 1.93E-04 -3.98E-03 **-1.31E-02** 1.12E-03 2.84E-03 3.80E-04 1.19E-02
6	-6 -5 -4 -3 -2 -1 **0** 1 2 3 4 5 6	8.76E-06 2.18E-04 3.53E-05 1.01E-04 7.92E-05 3.70E-05 **3.91E-05** -7.52E-05 1.87E-05 -1.26E-04 -1.05E-04 6.45E-05 2.24E-04	-5.44E-06 4.48E-04 -7.40E-05 -1.07E-04 2.52E-05 5.36E-05 **4.16E-05** -6.03E-05 1.06E-05 2.04E-04 -3.52E-05 3.78E-04 -2.25E-04	8.29E-05 2.25E-04 4.93E-05 4.51E-05 5.80E-05 5.27E-06 **4.76E-05** -4.92E-05 1.98E-05 -1.29E-04 -8.54E-05 2.04E-05 2.68E-04	-5.01E-05 2.94E-05 1.30E-05 2.25E-05 4.38E-06 -3.55E-05 **4.28E-05** 5.92E-06 1.14E-05 1.02E-06 7.02E-05 -3.59E-05 -3.13E-04

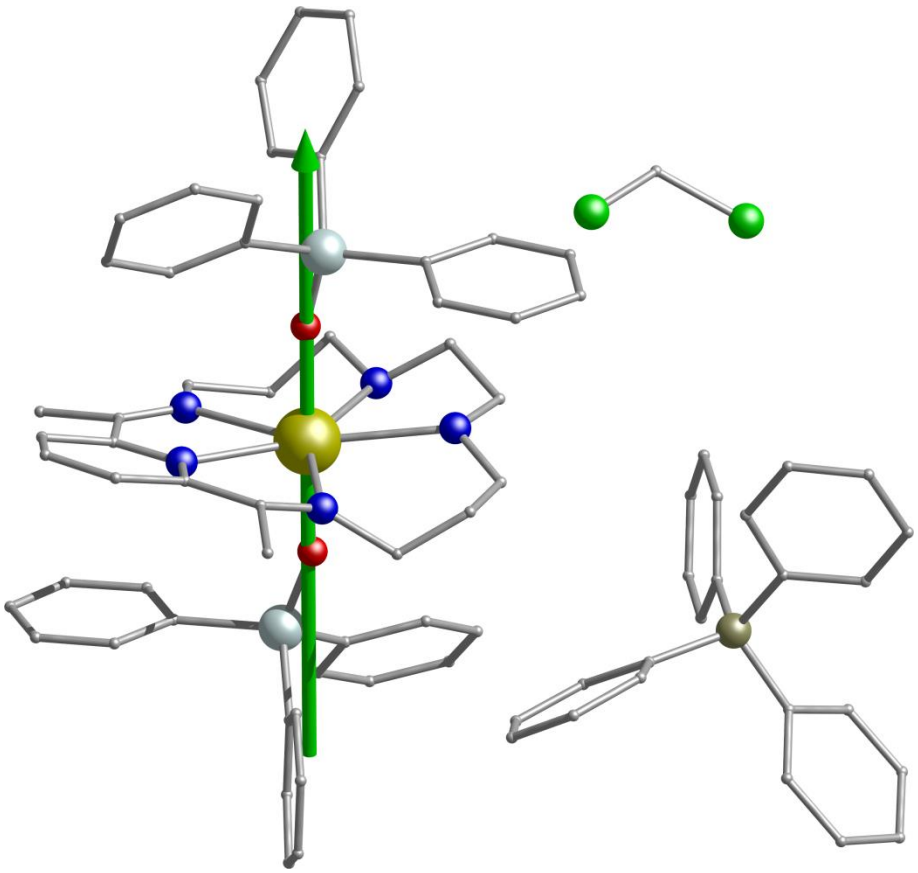

Fig. S13 *Ab initio* SINGLE_ANISO computed ground state Kramers Doublet for complex **1**. Colour code: Dy, gold; O, red; N, blue; Si, light turquoise; C, gray; B, dark yellow. Hydrogens are omitted for clarity.

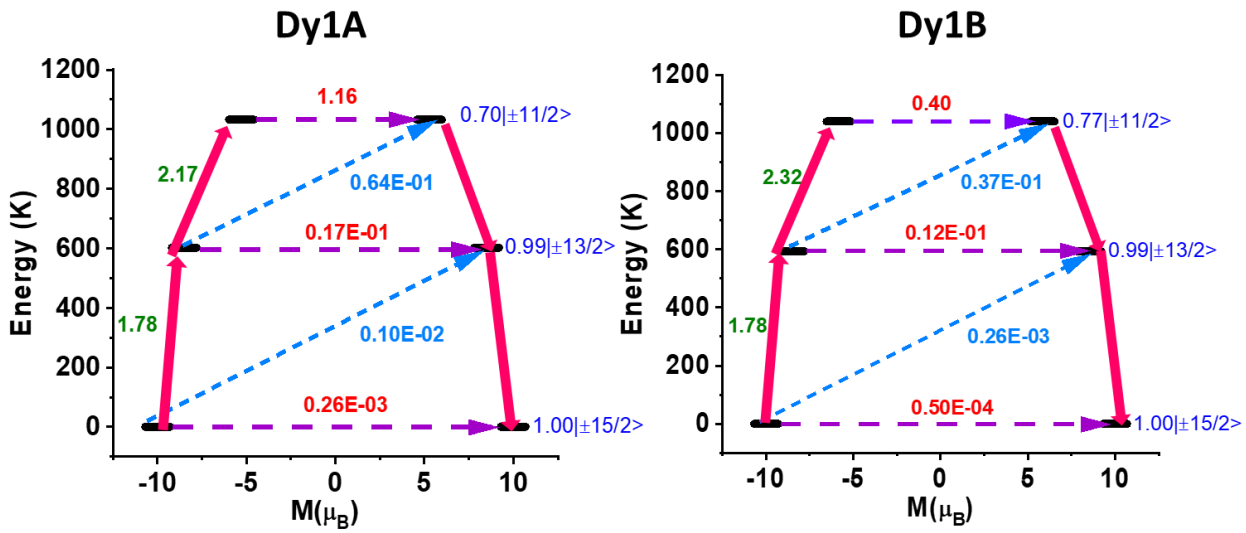

Fig. S14 *Ab initio* calculated relaxation dynamics for **1** calculated for both crystallographically independent Dy(III) centres (see main text). The arrows show the connected energy states with the number representing the matrix element of the transverse moment. Here, the black line indicates the KDs as function of magnetic moments. The violet dashed arrow represents QTM (QTM = quantum tunnelling of the magnetisation) via the ground state and TA-QTM (TA-QTM = thermally assisted QTM) via excited states. The blue dashed arrow indicates possible Orbach processes. The pink thick arrow indicates the mechanism of magnetic relaxation (Orbach/Raman). The numbers above each arrow represent corresponding transverse matrix elements for the transition magnetic moments.

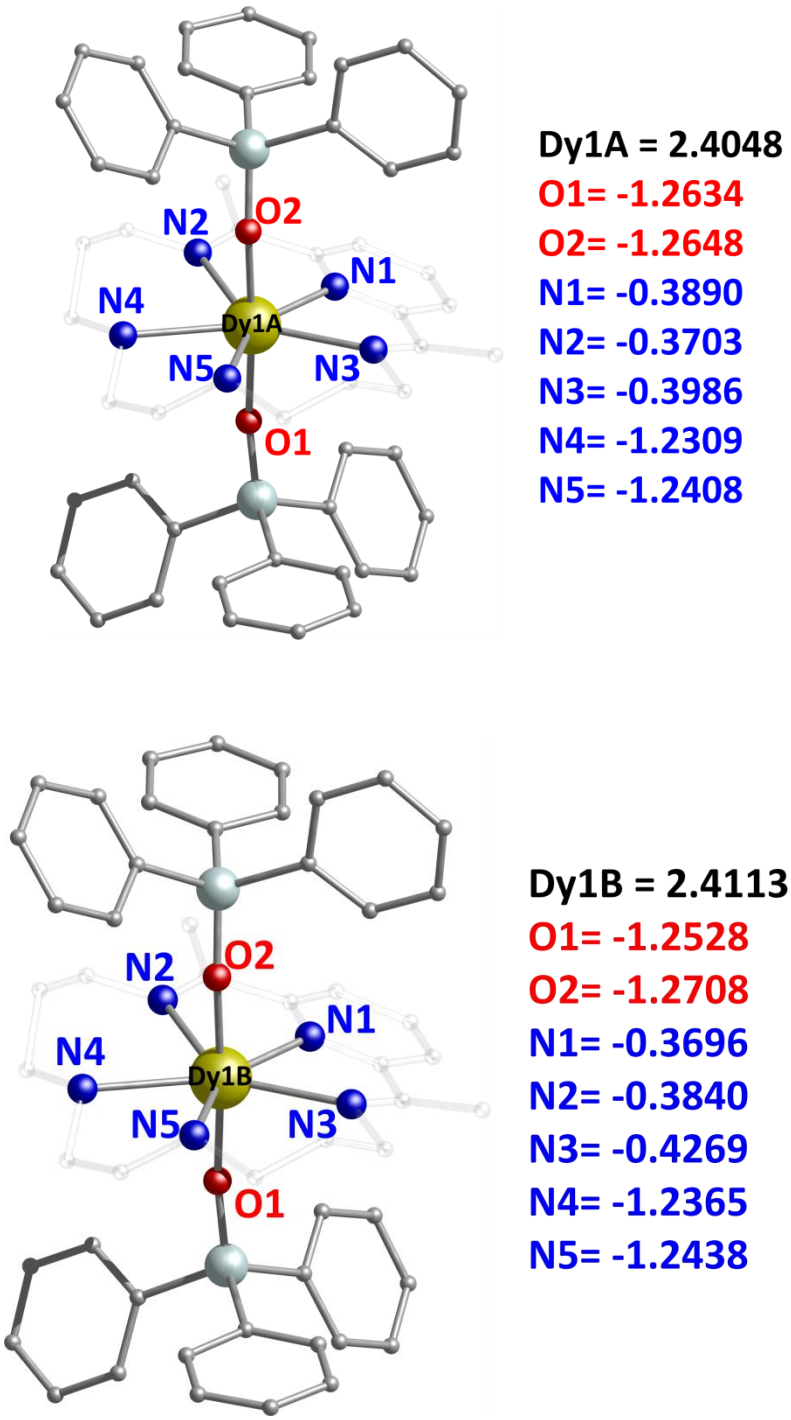

Fig. S15 LoProp charges of the atoms attached to the Dy(III) center for Dy1A (upper) and Dy1B (lower) in complex **1**. Colour code: Dy, gold; O, red; N, blue; Si, light blue; C, grey. Counter ion is omitted for clarity.[25]

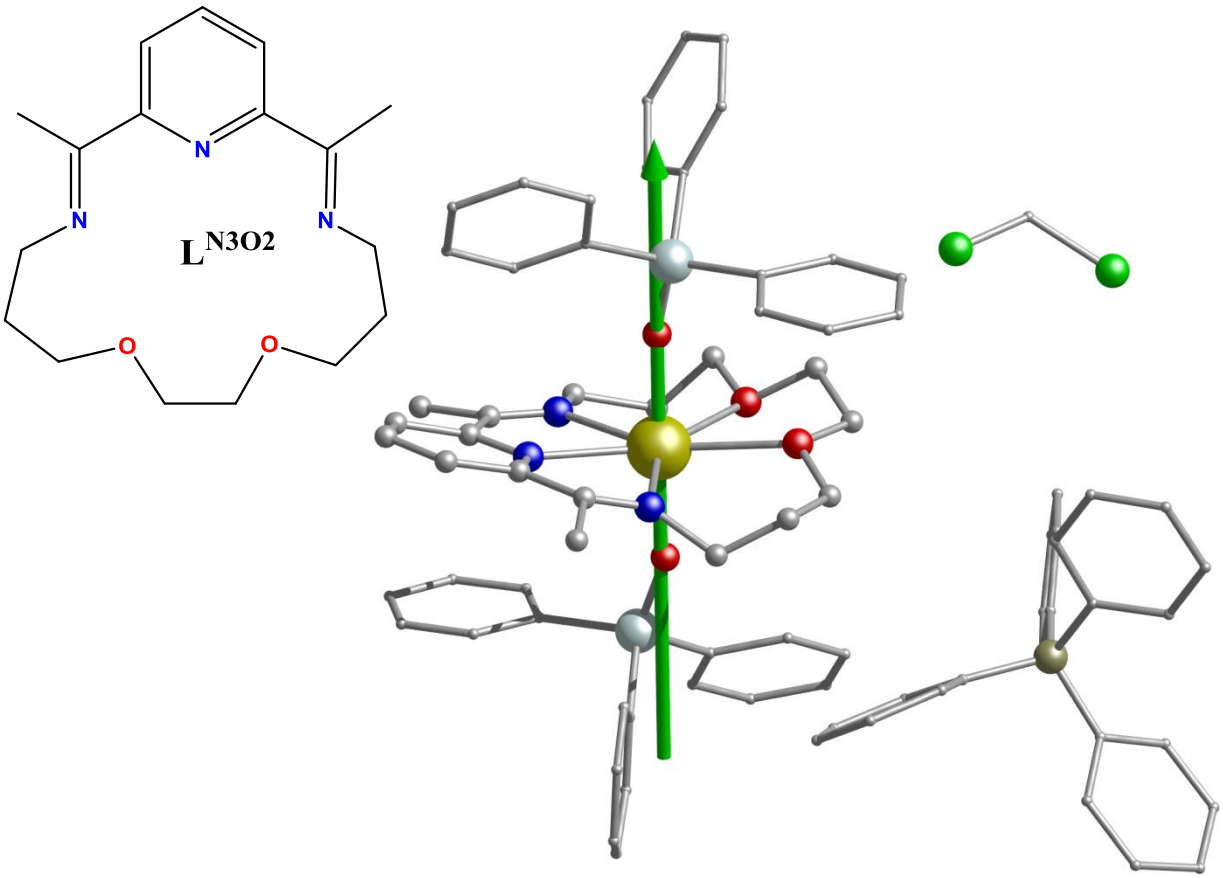

Fig. S16 *Ab initio* SINGLE_ANISO computed ground state Kramers Doublet for the model system **1-N3O2**. Inset: The new Schiff base ligand L^{N3O2} using linker 3,3'-(ethane-1,2-diylbis(oxy))bis(propan-1-amine) employed for model **1-N3O2**. Dy, gold; O, red; Si, light turquoise; C, gray. Hydrogens are omitted for clarity.

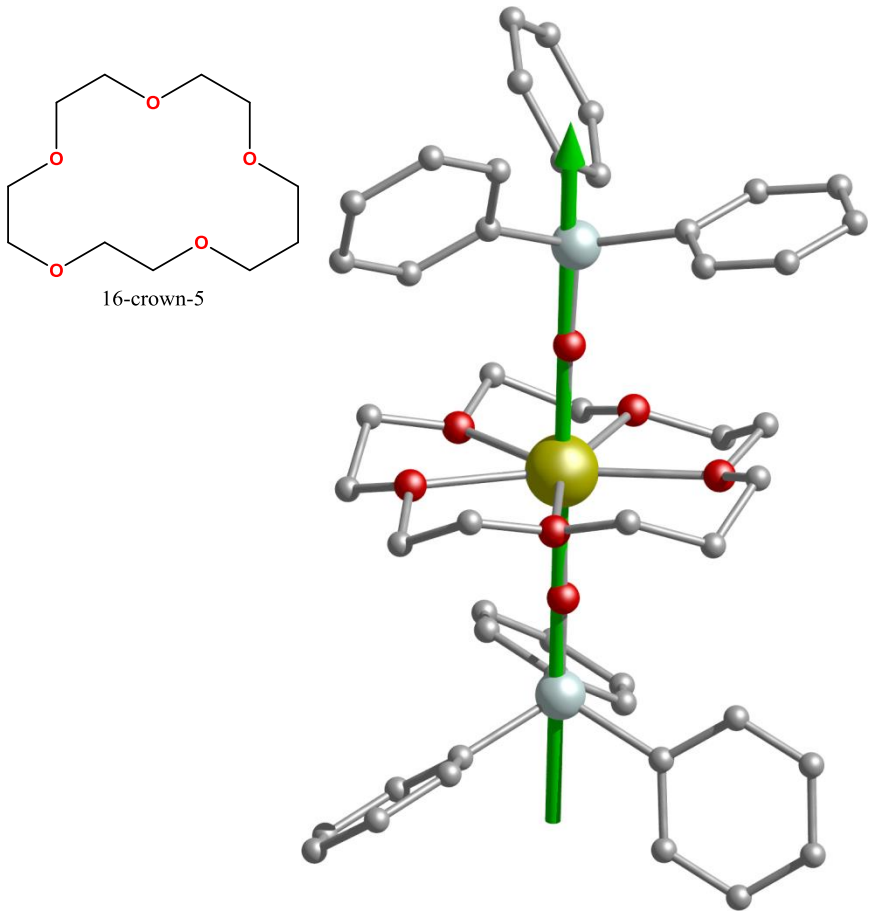

Fig. S17 *Ab initio* SINGLE_ANISO computed ground state Kramers Doublet for the model system **1-O5**. Inset: The 16-crown-5 ligand employed for model **1-O5**. Dy, gold; O, red; Si, light turquoise; C, gray. Hydrogens are omitted for clarity.

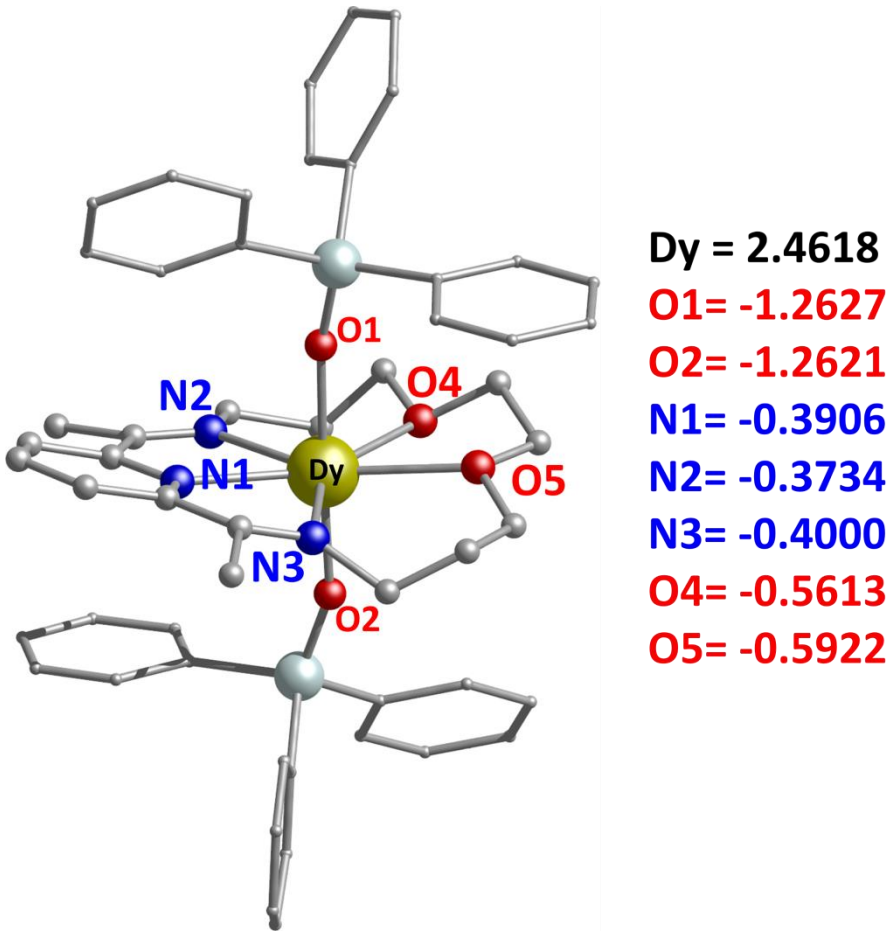

Fig. S18 LoProp charges of the atoms attached to the Dy(III) center for model system **1-N3O2**.[21] Colour code: Dy, gold; O, red; Si, light blue; C, grey. Counter ion is omitted for clarity.[25]

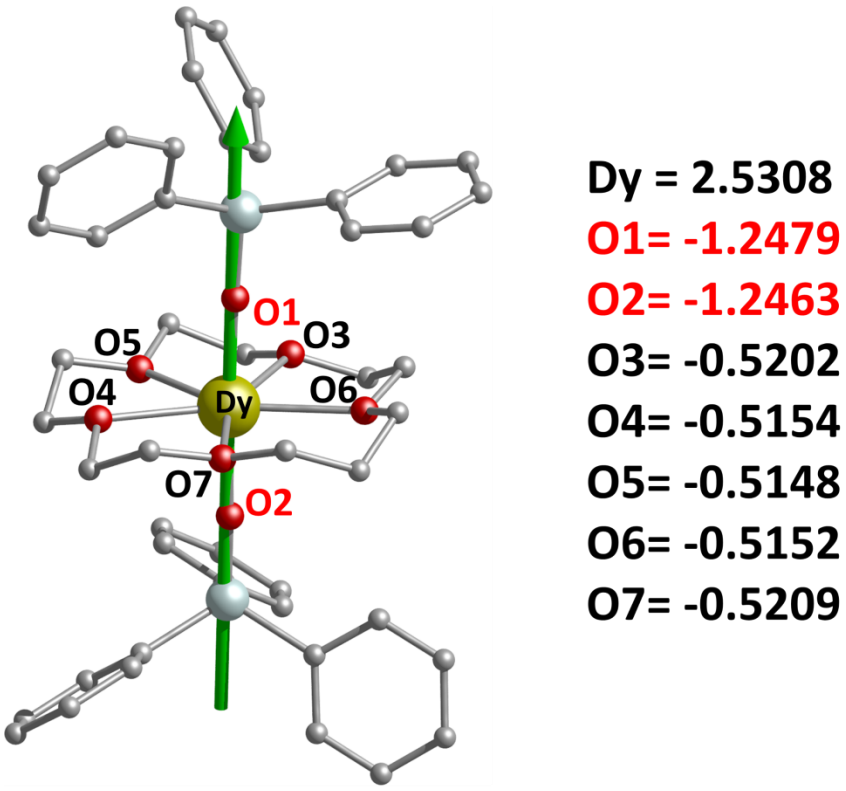

Fig. S19 LoProp charges of the atoms attached to the Dy(III) center for model system **1-O5**.[21] Colour code: Dy, gold; O, red; Si, light blue; C, grey. Counter ion is omitted for clarity.[25]

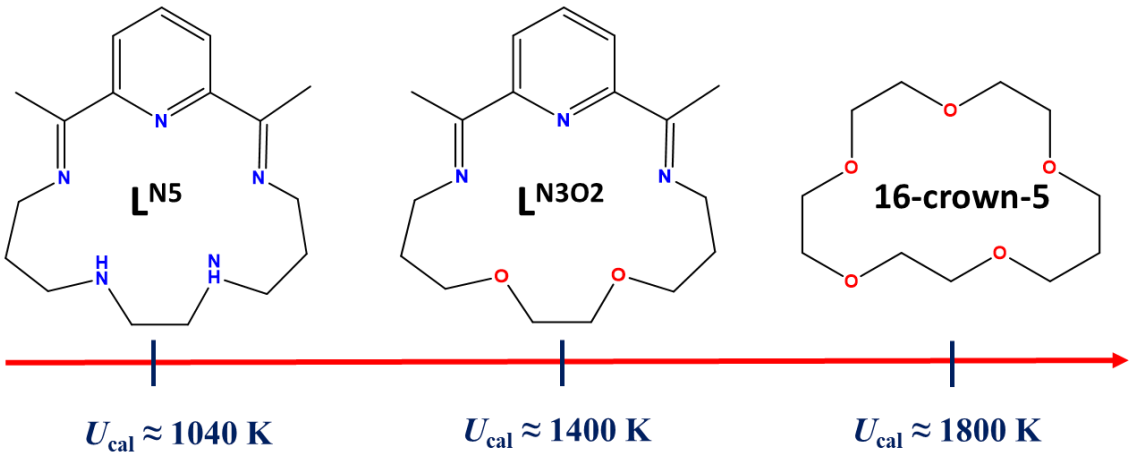

Fig. S20 Promising directions towards new pentagonal bipyramidal Dy(III) complexes using L^{N5}, L^{N3O2} and 16-crown-5 as equatorial ligands.

References

1 Y.-C. Chen, J.-L. Liu, L. Ungur, J. Liu, Q.-W. Li, L.-F. Wang, Z.-P. Ni, L. F. Chibotaru, X.-M. Chen and M.-L. Tong, *J. Am. Chem. Soc.*, 2016, **138**, 2829–2837.

2 S. K. Gupta, T. Rajeshkumar, G. Rajaraman and R. Murugavel, *Chem. Sci.*, 2016, **7**, 5181–5191.

3 J. Liu, Y.-C. Chen, J.-L. Liu, V. Vieru, L. Ungur, J.-H. Jia, L. F. Chibotaru, Y. Lan, W. Wernsdorfer, S. Gao, X.-M. Chen and M.-L. Tong, *J. Am. Chem. Soc.*, 2016, **138**, 5441–5450.

4 Y.-S. Ding, N. F. Chilton, R. E. P. Winpenny and Y.-Z. Zheng, *Angew. Chemie Int. Ed.*, 2016, **55**, 16071–16074.

5 Z. Jiang, L. Sun, Q. Yang, B. Yin, H. Ke, J. Han, Q. Wei, G. Xie and S. Chen, *J. Mater. Chem. C*, 2018, **6**, 4273–4280.

6 M. Li, H. Wu, Q. Yang, H. Ke, B. Yin, Q. Shi, W. Wang, Q. Wei, G. Xie and S. Chen, *Chem. – A Eur. J.*, 2017, **23**, 17775–17787.

7 A. B. Canaj, M. K. Singh, C. Wilson, G. Rajaraman and M. Murrie, *Chem. Commun.*, 2018, **54**, 8273–8276.

8 J. Long, A. N. Selikhov, E. Mamontova, K. A. Lyssenko, Y. Guari, J. Larionova and A. A. Trifonov, *Dalt. Trans.*, 2019, **48**, 35–39.

9 H. Wu, M. Li, B. Yin, Z. Xia, H. Ke, Q. Wei, G. Xie, S. Chen and S. Gao, *Dalt. Trans.*, 2019, **48**, 16384–16394.

10 I. F. Diáz-Ortega, J. M. Herrera, S. Dey, H. Nojiri, G. Rajaraman and E. Colacio, *Inorg. Chem. Front.*, 2020, **7**, 689–699.

11 Y. S. Ding, K. X. Yu, D. Reta, F. Ortu, R. E. P. Winpenny, Y. Z. Zheng and N. F. Chilton, *Nat. Commun.*, 2018, **9**, 3134.

12 Y. N. Guo, L. Ungur, G. E. Granroth, A. K. Powell, C. Wu, S. E. Nagler, J. Tang, L. F. Chibotaru and D. Cui, *Sci. Rep.*, 2014, **4**, 5471.

13 Y. S. Ding, T. Han, Y. Q. Zhai, D. Reta, N. F. Chilton, R. E. P. Winpenny and Y. Z. Zheng, *Chem. - A*

Eur. J., 2020, **26**, 5893–5902.

14 J. L. Liu, Y. C. Chen, Y. Z. Zheng, W. Q. Lin, L. Ungur, W. Wernsdorfer, L. F. Chibotaru and M. L. Tong, *Chem. Sci.*, 2013, **4**, 3310–3316.

15 P. E. Kazin, M. A. Zykin, V. V. Utochnikova, O. V. Magdysyuk, A. V. Vasiliev, Y. V. Zubavichus, W. Schnelle, C. Felser and M. Jansen, *Angew. Chemie - Int. Ed.*, 2017, **56**, 13416–13420.

16 M. Pinsky and D. Avnir, *Inorg. Chem.*, 1998, **37**, 5575–5582; D. Casanova, P. Alemany, J. M. Bofill and S. Alvarez, *Chem. - A Eur. J.*, 2003, **9**, 1281–1295; D. Casanova, J. Cirera, M. Llunell, P. Alemany, D. Avnir and S. Alvarez, *J. Am. Chem. Soc.*, 2004, **126**, 1755–1763.

17 D. Gatteschi, R. Sessoli and J. Villain, Molecular Nanomagnets, Oxford Univ. Press, 2006.

18 F. Aquilante, J. Autschbach, R. K. Carlson, L. F. Chibotaru, M. G. Delcey, L. De Vico, I. Fdez. Galván, N. Ferré, L. M. Frutos, L. Gagliardi, M. Garavelli, A. Giussani, C. E. Hoyer, G. Li Manni, H. Lischka, D. Ma, P. Å. Malmqvist, T. Müller, A. Nenov, M. Olivucci, T. B. Pedersen, D. Peng, F. Plasser, B. Pritchard, M. Reiher, I. Rivalta, I. Schapiro, J. Segarra-Martí, M. Stenrup, D. G. Truhlar, L. Ungur, A. Valentini, S. Vancoillie, V. Veryazov, V. P. Vysotskiy, O. Weingart, F. Zapata and R. Lindh, *J. Comput. Chem.*, 2016, **37**, 506–541.

19 P. Kalita, N. Ahmed, A. Kumar Bar, S. Dey, A. Jana, G. Rajaraman, J.-P. Sutter and V. Chandrasekhar, *Inorg. Chem.*, 2020, **59**, 6603–6612.

20 J. Mao, Z. Jin, J. Ni and L. Yu, *Polyhedron*, 1994, **13**, 313–317.

21 A. D. Becke, *J. Chem. Phys.*,1993, **98**, 5648.

22 Gaussian 09, Revision A.02, M. J. Frisch, G. W. Trucks, H. B. Schlegel, G. E. Scuseria, M. A. Robb, J. R. Cheeseman, G. Scalmani, V. Barone, B. Mennucci, G. A. Petersson, H. Nakatsuji, M. Caricato, X. Li, H. P. Hratchian, A. F. Izmaylov, J. Bloino, G. Zheng, J. L. Sonnenberg, M. Hada, M. Ehara, K. Toyota, R. Fukuda, J. Hasegawa, M. Ishida, T. Nakajima, Y. Honda, O. Kitao, H. Nakai, T. Vreven, J. A. Montgomery, Jr., J. E. Peralta, F. Ogliaro, M. Bearpark, J. J. Heyd, E. Brothers, K. N. Kudin, V. N. Staroverov, R. Kobayashi, J. Normand, K. Raghavachari, A. Rendell, J. C. Burant, S. S. Iyengar, J. Tomasi, M. Cossi, N. Rega, J. M. Millam, M. Klene, J. E. Knox, J. B. Cross, V. Bakken, C. Adamo, J. Jaramillo, R. Gomperts, R. E. Stratmann, O. Yazyev, A. J. Austin, R. Cammi, C. Pomelli, J. W. Ochterski, R. L. Martin, K. Morokuma, V. G. Zakrzewski, G. A. Voth, P. Salvador, J. J. Dannenberg, S. Dapprich, A. D. Daniels, O. Farkas, J. B. Foresman, J. V. Ortiz, J. Cioslowski and D. J. Fox, Gaussian, Inc., Wallingford CT, 2009.

23 T. R. Cundari and W. J.Stevens, *J. Chem. Phys.* 1993, 98, 5555−5565.

24 A. Schäfer, H. Horn and R. Ahlrichs, *J. Chem. Phys*.,1992, **97**, 2571; A. Schäfer, C. Huber and R. Ahlrichs, *J. Chem. Phys.,*1994,**100**, 5829.

25 L. Gagliardi, R. Lindh and G. Karlstrom, *J. Chem. Phys*., 2004, **121**, 4494.